Cell Reports

Sarbecovirus ORF6 proteins hamper induction of interferon signaling

Graphical abstract

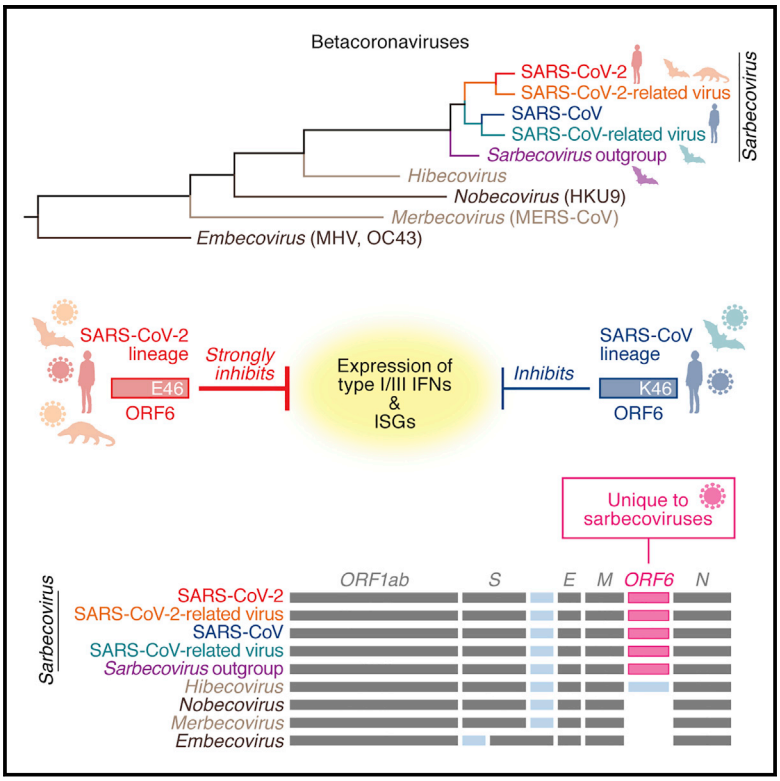

Highlights

- SARS-CoV-2 ORF6 inhibits innate immune signaling via its C-terminal region
- ORF6 proteins of SARS-CoV-2 lineages are more potent than those of SARS-CoV
- Residues E46 and Q56 determine the anti-interferon activity of ORF6
- The ORF6 gene is truncated C-terminally in ~0.2% of SARS-CoV-2 isolates

Authors

Izumi Kimura, Yoriyuki Konno, Keiya Uriu, Kristina Hopfensperger, Daniel Sauter, So Nakagawa, Kei Sato

Correspondence

keisato@g.ecc.u-tokyo.ac.jp

In brief

Kimura et al. show that the coronavirus *ORF6* gene encodes an interferon antagonist and is unique to sarbecoviruses, including SARS-CoV-2. Although the antagonistic activity of SARS-CoV-2 ORF6 depends on its C-terminal region, approximately 0.2% of all SARS-CoV-2 genomes isolated during the current COVID-19 pandemic harbor premature stop codons in *ORF6*.

Kimura et al., 2021, Cell Reports *34*, 108916
March 30, 2021
https://doi.org/10.1016/j.celrep.2021.108916

CellPress

Cell Reports

CellPress
OPEN ACCESS

Report

Sarbecovirus ORF6 proteins hamper induction of interferon signaling

Izumi Kimura,[1] Yoriyuki Konno,[1] Keiya Uriu,[1,2] Kristina Hopfensperger,[3,4] Daniel Sauter,[3,4] So Nakagawa,[5,6] and Kei Sato[1,6,7,8,*]

[1]Division of Systems Virology, Department of Infectious Disease Control, International Research Center for Infectious Diseases, Institute of Medical Science, The University of Tokyo, Tokyo 1088639, Japan
[2]Graduate School of Medicine, The University of Tokyo, Tokyo 1130033, Japan
[3]Institute of Molecular Virology, Ulm University Medical Center, Ulm 89081, Germany
[4]Institute for Medical Virology and Epidemiology of Viral Diseases, University Hospital Tübingen, Tübingen 72076, Germany
[5]Department of Molecular Life Science, Tokai University School of Medicine, Kanagawa 2591193, Japan
[6]CREST, Japan Science and Technology Agency, Saitama 3220012, Japan
[7]Twitter: @SystemsVirology
[8]Lead contact
*Correspondence: keisato@g.ecc.u-tokyo.ac.jp
https://doi.org/10.1016/j.celrep.2021.108916

SUMMARY

The presence of an *ORF6* gene distinguishes sarbecoviruses such as severe acute respiratory syndrome coronavirus (SARS-CoV) and SARS-CoV-2 from other betacoronaviruses. Here we show that ORF6 inhibits induction of innate immune signaling, including upregulation of type I interferon (IFN) upon viral infection as well as type I and III IFN signaling. Intriguingly, ORF6 proteins from SARS-CoV-2 lineages are more efficient antagonists of innate immunity than their orthologs from SARS-CoV lineages. Mutational analyses identified residues E46 and Q56 as important determinants of the antagonistic activity of SARS-CoV-2 ORF6. Moreover, we show that the anti-innate immune activity of ORF6 depends on its C-terminal region and that ORF6 inhibits nuclear translocation of IRF3. Finally, we identify naturally occurring frameshift/nonsense mutations that result in an inactivating truncation of ORF6 in approximately 0.2% of SARS-CoV-2 isolates. Our findings suggest that ORF6 contributes to the poor IFN activation observed in individuals with coronavirus disease 2019 (COVID-19).

INTRODUCTION

An unusual outbreak of infectious pneumonia in Wuhan, Hubei Province, China, was first reported in December 2019. Within a few weeks, a novel coronavirus (CoV) was identified as the causative agent of this infectious disease, CoV disease 2019 (COVID-19) (Zhou et al., 2020b). Because this virus is phylogenetically related to severe acute respiratory syndrome (SARS)-CoV, it was called SARS-CoV-2. As of January 2021, SARS-CoV-2 is an ongoing pandemic; approximately 100 million cases of SARS-CoV-2 infection have been reported worldwide, and more than two million people have died of COVID-19 (WHO, 2020). Therefore, a better understanding of SARS-CoV-2 infection and pathogenesis is urgently needed.

SARS-CoV and SARS-CoV-2 are closely related, both belong to the family Coronaviridae, genus *Betacoronavirus* and subgenus *Sarbecovirus* (Lam et al., 2020; Zhou et al., 2020b). SARS-CoV-related viruses have been detected in palm civets (*Paguma larvata*) (Wang et al., 2005), Chinese rufous horseshoe bats (*Rhinolophus sinicus*) (Lau et al., 2005; Li et al., 2005), and a variety of additional bat species (mainly of the genus *Rhinolophus*) (Ge et al., 2013; He et al., 2014; Hu et al., 2017; Lau et al., 2010; Lin et al., 2017; Tang et al., 2006; Wang et al., 2017; Wu et al., 2016b; Yuan et al., 2010). Similarly, SARS-CoV-2-related viruses have been identified in intermediate horseshoe bats (*Rhinolophus affinis*) (Zhou et al., 2020b) and a Malayan horseshoe bat (*Rhinolophus malayanus*) (Zhou et al., 2020a) as well as Malayan pangolins (*Manis javanica*) (Lam et al., 2020; Xiao et al., 2020). This suggests that zoonotic viral transmission from horseshoe bats to humans led to emergence of human pathogenic sarbecoviruses, including SARS-CoV and SARS-CoV-2.

In addition to sarbecoviruses, other human pathogenic betacoronaviruses have been reported. Middle East respiratory syndrome (MERS)-CoV belongs to the subgenus *Merbecovirus* (van Boheemen et al., 2012; Zaki et al., 2012), whereas the human CoVs OC43 (McIntosh et al., 1967) and HKU1 (Woo et al., 2005) belong to the subgenus *Embecovirus*. Non-human betacoronaviruses have also been reported; HKU4 and HKU5 are included in the subgenus *Merbecovirus* (Woo et al., 2007), whereas murine hepatitis virus (MHV) belonging to *Embecovirus* is a pathogenic CoV in mice (Lai et al., 1981; Spaan et al., 1988). Some CoVs classified in the subgenus *Hibecovirus* have been detected in bats (Quan et al., 2010; Wu et al., 2016a, 2016b) but have not yet been found in humans. Human

betacoronaviruses are not only phylogenetically related but also cause similar respiratory symptoms, such as cough and pneumonia (reviewed in Chan-Yeung and Xu, 2003; Weiss, 2020). Nevertheless, they differ significantly in their pathogenicity and severity of infection. For instance, SARS-CoV (WHO, 2004) and MERS-CoV (WHO, 2019) are highly pathogenic, whereas OC43 and HKU1 cause relatively mild diseases (reviewed in Chan-Yeung and Xu, 2003; Perlman and Masters, 2020; Weiss, 2020). These features suggest that direct comparison of their genome structure and the functions of their viral proteins will help us understand determinants of disease.

A clear difference between COVID-19 and SARS in terms of immune responses is the limited induction of type I interferon (IFN-I; e.g., IFN-α) and type III IFN (IFN-III; e.g., IFN-λ3) upon SARS-CoV-2 infection compared with SARS-CoV infection (Blanco-Melo et al., 2020; Hadjadj et al., 2020). Importantly, impaired IFN-I/III responses define a high-risk population of individuals with COVID-19 (Hadjadj et al., 2020), and this immunological feature may be an important determinant of the pathogenesis of SARS-CoV-2 infection. As a factor that potentially contributes to insufficient IFN activation in SARS-CoV-2-infected individuals, we recently identified the viral ORF3b protein (Konno et al., 2020). Additionally, recent studies have revealed that SARS-CoV-2-encoded proteins such as NSP1, NSP12, nucleoprotein (N), and ORF6 potentially impair IFN activation (Lei et al., 2020; Li et al., 2020a; Miorin et al., 2020; Xia et al., 2020; Yuen et al., 2020), with ORF6 being one of the most potent IFN antagonists (Hayn et al., 2020; Lei et al., 2020; Xia et al., 2020).

In the present study, we show that an *ORF6* gene is commonly encoded in all sarbecoviruses, including SARS-CoV and SARS-CoV-2, whereas no orthologs are found in other betacoronaviruses, such as MERS-CoV, OC43, and MHV. We demonstrate that all *Sarbecovirus* ORF6 proteins inhibit induction of IFN-I upon viral infection as well as antiviral signaling triggered by IFN-I/III. Intriguingly, the anti-IFN activities of the ORF6 proteins of SARS-CoV-2 lineages are more potent than those of SARS-CoV lineages. We further provide evidence suggesting that the emergence of SARS-CoV-2 variants expressing truncated ORF6 proteins may contribute to attenuation of viral pathogenicity.

RESULTS

ORF6 is conserved in the subgenus *Sarbecovirus* but absent from other betacoronaviruses

We first assessed the phylogenetic relationship of betacoronaviruses, including SARS-CoV, SARS-CoV-2, MERS-CoV, OC43, and HKU1. The respective viral strains were classified based on their subgenera in the phylogenetic tree of the full-length viral genome (Figure 1A; Table S1) as well as five viral core genes encoding ORF1ab, spike (S), envelope (E), membrane protein (M), and N (Figure 1B). The inconsistent phylogenetic topologies of different viral genes of sarbecoviruses (Figure 1B) are in agreement with recent studies suggesting gene recombination events among sarbecoviruses (Boni et al., 2020; Li et al., 2020b). However, some viral core genes such as *E* (encoding 75 amino acids in the case of SARS-CoV-2) are relatively short, making it difficult to reliably infer their phylogenetic relationships. Indeed, two viruses belonging to the *Sarbecovirus* outgroup, BtKY72 and BM48, were separated in the phylogenetic tree of the *E* gene (Figure 1B). In contrast, the other six phylogenetic trees showed almost identical relationships among the five subgenera of betacoronaviruses (Figures 1A and 1B). These results suggest that viral recombination did not occur among the analyzed betacoronaviruses, although recombination events can occur among sarbecoviruses.

We then compared the genome organizations of the different subgenera. As shown in Figure 1C, the arrangement of the core genes (*ORF1ab-S-E-M-N*) is conserved. Insertions of additional open reading frames (ORFs) between *ORF1ab* and *S* were detected in *Hibecovirus* (Hp/Zhejuang2013) and *Embecovirus* species, whereas additional ORFs were detected between *S* and *E* in all betacoronaviruses (Figure 1C). Interestingly, ORF insertions between *M* and *N* were observed only in members of the *Sarbecovirus* and *Hibecovirus* subgenera (Figure 1C). When we compared the sequences of these ORFs, the genes in *Sarbecovirus* were unalignable with those in *Hibecovirus*, suggesting that these ORFs emerged independently after the divergence of these subgenera. Of note, we found that *ORF6* is highly conserved in sarbecoviruses, including SARS-CoV and SARS-CoV-2, but absent from other betacoronaviruses (Figure 1C).

ORF6 proteins of SARS-CoV-2 lineages inhibit activation of IFN signaling more potently than those of SARS-CoV lineages

Because previous reports have suggested that SARS-CoV ORF6 has the ability to inhibit IFN-I activation as well as upregulation of IFN-stimulated genes (ISGs) (Frieman et al., 2007; Kopecky-Bromberg et al., 2007), we directly compared the phenotypic properties of representative *Sarbecovirus* ORF6 proteins. The phylogenetic topology of the *Sarbecovirus ORF6* gene (Figure 2A) was similar to that of the full-length viral genome (Figure 1A), suggesting that recombination events involving the *ORF6* gene have not occurred among sarbecoviruses. For our phenotypic analyses, we generated expression plasmids for ORF6 from SARS-CoV-2 (Wuhan-Hu-1) as well as SARS-CoV-2-related viruses from bats (RmYN02, RaTG13, and ZXC21) and a pangolin (P4L). We also included ORF6 from SARS-CoV (Tor2), SARS-CoV-related viruses from bats (Rs4231, Rm1, and HKU3-2), and the two bat sarbecoviruses that are phylogenetically located at the outgroup of SARS-CoV-2 and SARS-CoV (BtKY72 and BM48). Western blotting revealed that the expression levels of ORF6 proteins of the SARS-CoV-2 lineage are lower than those of the SARS-CoV lineage and the two outgroup viruses (Figure 2B).

We then monitored human *IFNB1* promoter activity in the presence of ORF6 using a luciferase reporter assay. Influenza A virus (IAV) non-structural protein 1 (NS1) served as a positive control because it potently suppresses induction of *IFNB1* (García-Sastre et al., 1998; Krug et al., 2003). As shown in Figure 2C, top, all ORF6 proteins as well as IAV NS1 dose-dependently suppressed activation of the *IFNB1* promoter upon Sendai virus (SeV) infection. Notably, ORF6 proteins of the SARS-CoV-2 lineage were more potent inhibitors than those of the SARS-CoV lineage (Figure 2C, top), despite their lower expression levels (Figure 2B). Next we analyzed the ORF6 proteins for their ability

CellPress
OPEN ACCESS

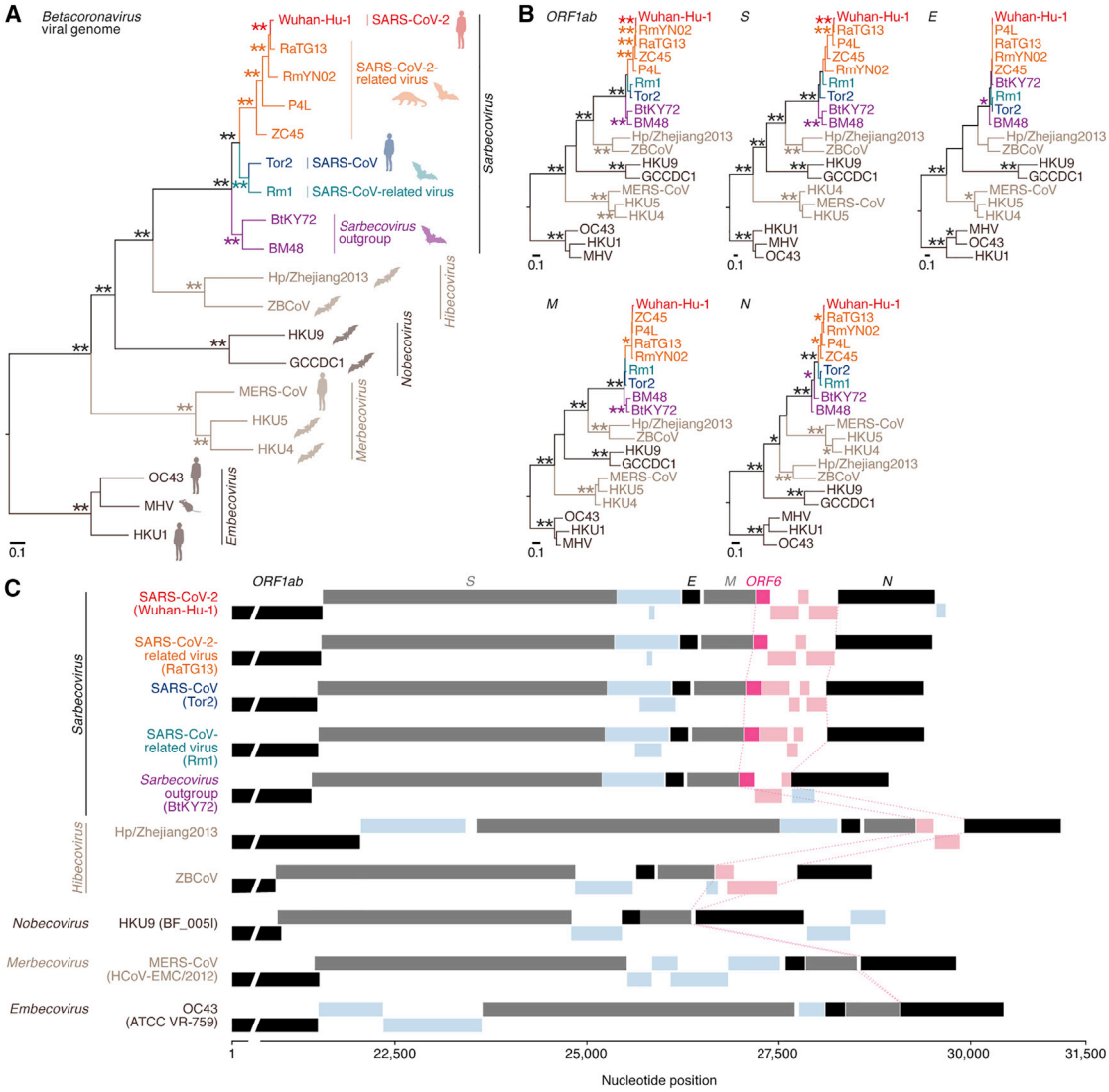

Figure 1. Phylogenetic relationship and gene structure of betacoronaviruses

(A and B) Maximum likelihood phylogenetic trees of full-length betacoronavirus sequences (A) and five core genes (*ORF1ab*, *S*, *E*, *M*, and *N*) (B). Accession numbers, strain names, and host species are summarized in Table S1. A scale bar indicates 0.1 substitutions per site. Bootstrap values; **, > 95%; *, > 75%. (C) Gene structure of betacoronaviruses. The five core genes (*ORF1ab*, *S*, *E*, *M*, and *N*) are indicated by black or gray, whereas the inserted ORFs are indicated in blue. The ORFs inserted between *M* and *N* are shown in light pink, and *Sarbecovirus ORF6* genes are shown in pink. The end site of *M* and the start site of *N* are connected by broken pink lines. Representative strains of the respective subgenera are indicated in parentheses.
See also Table S1.

to inhibit signaling triggered by IFN-I (IFN-α) and IFN-III (IFN-λ3). In agreement with a previous study (Kochs et al., 2007), IAV NS1 failed to prevent activation of the IFN-stimulated response element (ISRE) promoter upon stimulation with IFN-I or IFN-III (Figure 2C, center and bottom). In contrast, *Sarbecovirus* ORF6 proteins inhibited activation of the ISRE promoter upon IFN-I and IFN-III stimulation (Figure 2C, center and bottom). Notably, ORF6 proteins of the SARS-CoV-2 lineage were again more active than those of the SARS-CoV lineage (Figure 2C, center and bottom). Thus, our data demonstrate that SARS-CoV-2 ORF6 is a potent IFN antagonist that targets signaling triggered by SeV infection (leading to *IFNB1* expression) and IFN-α and IFN-λ3 stimulation (leading to ISG expression). In addition to the ORF6 proteins of SARS-CoV and SARS-CoV-2, the ORF6 proteins of the two outgroups, BtKY72 and BM48, significantly inhibited these antiviral signaling cascades, with BtKY72 ORF6 being less efficient than BM48 ORF6 (Figure 2C). Two recent reports suggested that the compounds ivermectin (Caly et al., 2020) and selinexor (Gordon et al., 2020) may be candidates for treatment of COVID-19 as they target the activity of ORF6. However, both compounds failed to inhibit the anti-IFN activity of ORF6 (Figure S1A).

To verify the immunosuppressive activity of ORF6 in different experimental systems, the expression levels of endogenous

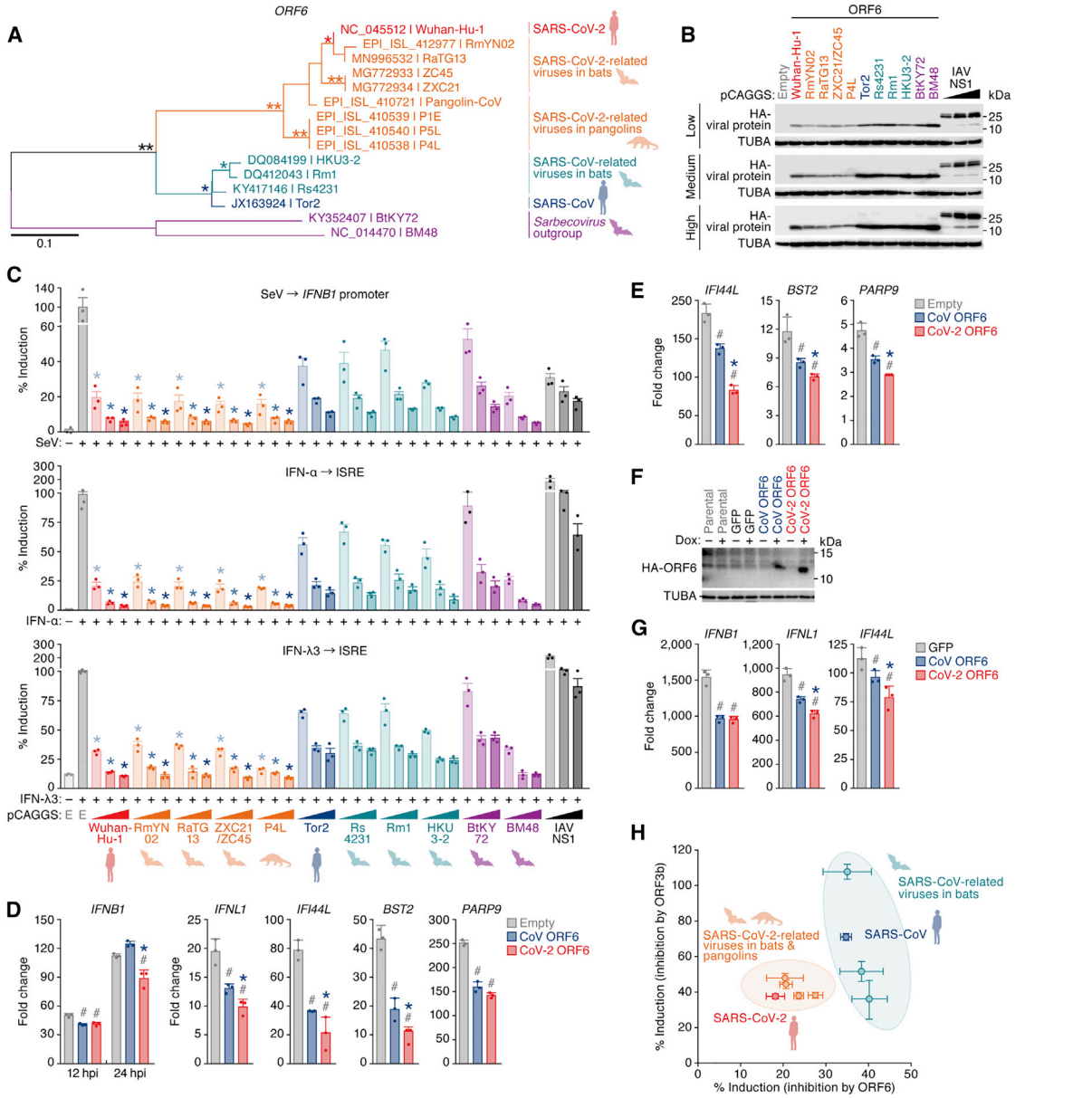

Figure 2. Potent anti-innate immune signaling activity of *Sarbecovirus* ORF6

(A) A maximum likelihood phylogenetic tree of *Sarbecovirus ORF6* sequences. Accession number, strain name, and the host of each virus are indicated. A scale bar indicates 0.1 nucleotide substitutions per site. Bootstrap values; **, > 95%; *, > 75%.

(B and C) Potent anti-IFN activity of *Sarbecovirus* ORF6. HEK293 cells were cotransfected with three different amounts of plasmids expressing hemagglutinin (HA)-tagged *Sarbecovirus* ORF6 or IAV NS1 and p125Luc (C, top) or pISRE-luc (C, center and bottom). 24 h after transfection, cells were infected with SeV (MOI 10) (C, top) or treated with IFN-α (C, center) or IFN-λ3 (C, bottom). 24 h after infection or treatment, cells were harvested for western blotting (B) and a luciferase assay (C). Note that the *ORF6* sequence of ZXC21 is identical to that of ZC45. In (B), "low," "medium," and "high" indicate the amount of transfected *Sarbecovirus* ORF6 expression plasmids.

(D and E) Anti-innate immune signaling activity of SARS-CoV-2 ORF6 in HEK293 cells. HEK293 cells were transfected with plasmids expressing HA-tagged ORF6. 24 h after transfection, cells were infected with SeV (MOI 10) (D) or treated with IFN-α (E). 12 h (*IFNB1* only) or 24 h (all genes) after infection (D) or 8 h after IFN-α treatment (E), endogenous expression levels of the indicated genes were measured by real-time RT-PCR.

(F and G) Anti-IFN activity of SARS-CoV-2 ORF6 in lung cells.

(F) Expression of HA-tagged ORF6 upon Dox stimulation.

(G) A549 cells stably transduced with a Dox-inducible HA-tagged ORF6 or GFP (F) were treated with Dox and infected with SeV (MOI 10). 4 h after infection, the endogenous expression levels of the indicated genes were measured by real-time RT-PCR.

(H) Comparison of the anti-IFN activity of *Sarbecovirus* ORF6 and ORF3b. The anti-IFN activities of ORF6 (100 ng, x axis) and ORF3b (100 ng, y axis) (Figures S1C and S1D) are summarized.

(legend continued on next page)

IFNB1, *IFNL1*, and three ISGs (*IFI44L*, *BST2*, and *PARP9*), were measured after SeV infection (Figure 2D) or IFN-α treatment (Figure 2E). The ORF6 proteins of SARS-CoV-2 and SARS-CoV significantly suppressed upregulation of these genes (Figures 2D and 2E). The suppressive effect mediated by SARS-CoV-2 ORF6 was significantly higher compared with its SARS-CoV counterpart (Figures 2D and 2E). To further validate the anti-IFN activity of ORF6 in a more physiological setting, we generated a derivative of the human lung cell line A549 expressing ORF6 upon doxycycline (Dox) treatment (Figure 2F) and monitored the expression levels of endogenous *IFNB1*, *IFNL1*, and *IFI44L* after SeV infection. Although the ORF6 expression level induced by Dox treatment in A549 cells was much lower than in transiently transfected HEK293 cells (Figure S1B), this approach revealed that ORF6 significantly suppresses induction of antiviral genes in relevant target cells of SARS-CoV-2 (Figure 2G). Moreover, we show that the anti-IFN activity of ORF6 is, on average, higher than that of ORF3b (Figures S1C and S1D), a recently identified IFN antagonist of SARS-CoV-2 (Konno et al., 2020). For both proteins, the anti-IFN activities tended to be higher in the SARS-CoV-2 lineage compared with the SARS-CoV lineage (Figure 2H). These findings identify SARS-CoV-2 ORF6 as a robust IFN antagonist.

E46 and Q56 determine the anti-innate immune activity of SARS-CoV-2 ORF6

Although all tested *Sarbecovirus* ORF6 proteins efficiently hampered induction of *IFNB1* triggered by SeV infection and upregulation of ISGs induced by IFN-I/III, the inhibitory activities of SARS-CoV-2 ORF6 were significantly stronger than those of SARS-CoV ORF6 (Figure 2). To determine the residue(s) that are responsible for this difference, we aligned and compared the ORF6 amino acid sequences (Figure S2A). As shown in Figure 3A, we found 10 amino acids whose chemical properties are different between ORF6 proteins of the SARS-CoV lineage (n = 241) and those of the SARS-CoV-2 lineage (n = 57,648), and these 10 residues are highly conserved in each lineage. Furthermore, the ORF6 proteins of the SARS-CoV lineage harbor two additional amino acids (i.e., Y and P) at the C terminus compared with those of the SARS-CoV-2 lineage. Mutational analysis (Figure 3B) revealed that substitution E46K attenuates the anti-IFN activity of SARS-CoV-2 ORF6, whereas Q56E has the opposite effect (Figures 3C and S2B). To verify the effect of residues 46 and 56 on ORF6-mediated anti-IFN activity, we introduced the respective reverse mutations into SARS-CoV ORF6 (Figure 3D). As shown in Figures 3E and S2C, the inhibitory activity of the SARS-CoV ORF6 K46E mutant was significantly higher than that of the parental SARS-CoV ORF6 protein, whereas the E56Q mutant of SARS-CoV ORF6 antagonizes IFN induction less efficiently than the parental SARS-CoV ORF6. These findings show that the differences in anti-IFN activity between SARS-CoV-2 ORF6 and its SARS-CoV counterpart are determined by these two residues.

Inhibition of innate immune signaling depends on the C-terminal region of *Sarbecovirus* ORF6

The observation that residues 46 and 56 determine the ability of ORF6 to inhibit responsiveness to viral infection and IFNs (Figures 3B–3E and S2C) suggests that ORF6 targets a step that is common to these signaling pathways. A comprehensive proteome analysis by Gordon et al. (2020) has suggested that ORF6 interacts with two cellular proteins, ribonucleic acid export 1 (RAE1) and nucleoporin 98 (NUP98), via its C-terminal region. To verify the importance of the C-terminal region of ORF6 for its biological activity, we generated a series of ORF6 mutants in which we deleted the C-terminal region or changed a stretch of positively charged residues to alanines (Figure 3F). With the exception of the ΔC1 mutant of SARS-CoV-2 (Wuhan-Hu-1), all mutants were expressed at levels similar to wild-type (WT) ORF6 (Figure 3G). Luciferase reporter assays revealed that deletion of the C-terminal region (ΔC2) or substitution of acidic residues to alanines (Ala) completely abrogated the anti-IFN effects of SARS-CoV-2 ORF6 (Figures 3H and S2D). Similarly, the anti-IFN activities of the ORF6 proteins of SARS-CoV (Tor2) and two outgroups (BtKY72 and BM48) were partially attenuated by mutations of the C-terminal region, although they still retained some of their anti-IFN activity (Figures 3H and S2D). These findings suggest that the C-terminal region is crucial for efficient anti-IFN activity of ORF6.

To address whether ORF6 interacts with RAE1 and NUP98 via its C-terminal region, we performed co-immunoprecipitation (coIP) experiments. As shown in Figure 3I, *Sarbecovirus* ORF6 proteins, including those of SARS-CoV-2 (Wuhan-Hu-1), SARS-CoV (Tor2), and two outgroups (BtKY72 and BM48), bound to RAE1 and NUP98. In contrast, C-terminally truncated mutants thereof failed to bind these cellular proteins (Figure 3I). These observations suggest that RAE1 and NUP98 associate with the anti-IFN-activity exerted by *Sarbecovirus* ORF6 proteins. In fact, a recent study demonstrated that SARS-CoV-2 ORF6 hampers nuclear translocation of IRF3 and STAT1 via RAE1 and NUP98 and suggested that overexpression of RAE1 and NUP98 rescues the IFN response in the presence of ORF6 (Miorin et al., 2020). Although our microscopy analyses (Figure 3J) confirmed that SARS-CoV-2 ORF6 inhibits nuclear translocation of IRF3 (Figure 3K), overexpression of RAE1 and NUP98 did not rescue nuclear translocation of IRF3 (Figures 3J and 3K),

For western blotting (B and F), the input of the cell lysate was normalized to TUBA, and one representative result of three independent experiments is shown. In (B), three different doses of IAV NS1 were used as controls on each membrane. kDa, kilodalton. For the luciferase assay (C), the value was normalized to the unstimulated, empty vector-transfected cells (no SeV infection in the top panel and no IFN treatment in the center and bottom panels). For real-time RT-PCR (D, E, and G), expression of the target gene was normalized to *GAPDH*, and the fold change to the value of 0 h is shown. For the luciferase assay (C) and real-time RT-PCR (D, E, and G), mean values of three independent experiments with SEM are shown. In (C), statistically significant differences ($p < 0.05$) compared with the same amount of SARS-CoV (Tor2) ORF6-transfected cells (*) are shown. In (D), (E), and (G), statistically significant differences ($p < 0.05$) compared with empty vector-transfected cells (#, D and E), GFP-expressing cells upon Dox stimulation (#, G), and SARS-CoV (Tor2) ORF6-transfected cells (*) are shown. E, empty vector.
See also Figure S1.

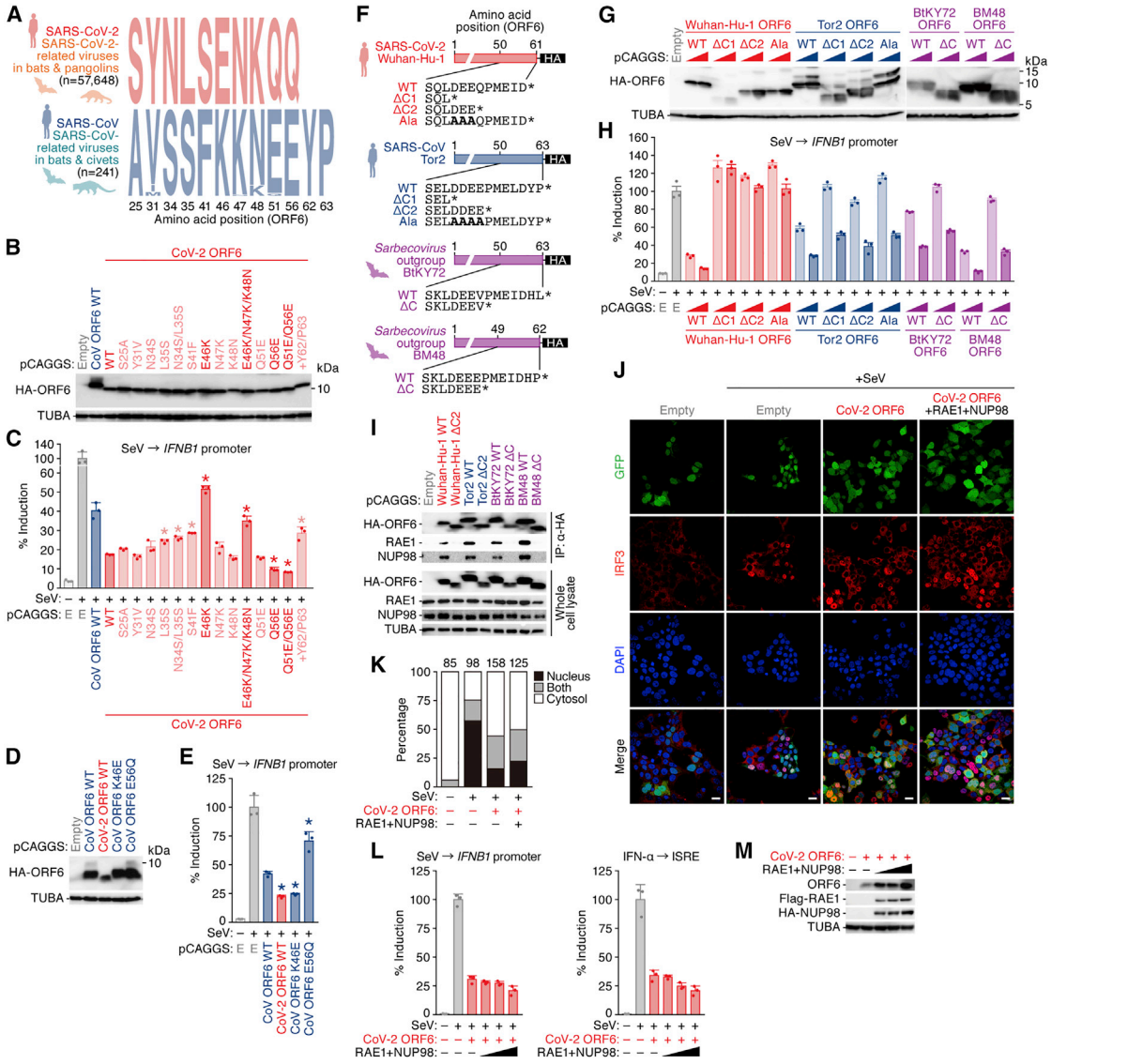

Figure 3. Mapping residues that determine the potent anti-innate immune signaling activity of SARS-CoV-2 ORF6

(A) Comparison of ORF6 residues that are different between the SARS-CoV-2 and SARS-CoV lineages. Numbers in parentheses indicate the total number of analyzed sequences. A comparison of all ORF6 residues is shown in Figure S2A.

(B–E) Anti-IFN activity of SARS-CoV-2 ORF6 mutants (B and C) and SARS-CoV ORF6 mutants (D and E). HEK293 cells were cotransfected with plasmids expressing HA-tagged ORF6 variants and p125Luc. 24 h after transfection, cells were infected with SeV (MOI 10). 24 h after infection, cells were harvested for western blotting (B and D) and a luciferase assay (C and E).

(F) Scheme illustrating the generated ORF6 C-terminal mutants.

(G and H) Anti-IFN activity of *Sarbecovirus* ORF6 mutants. HEK293 cells were cotransfected with plasmids expressing HA-tagged ORF6 variants and p125Luc. 24 h after transfection, cells were infected with SeV (MOI 10). 24 h after infection, cells were harvested for western blotting (G) and a luciferase assay (H).

(I) ORF6 interaction with RAE1 and NUP98. HEK293 cells were transfected with plasmids expressing HA-tagged ORF6 WT or the respective ΔC mutant (ΔC2 for SARS-CoV-2 Wuhan-Hu-1 and SARS-CoV Tor2), and coIP was performed as described in the STAR Methods.

(J and K) Subcellular localization of ORF6 and IRF3. HEK293T cells were transfected with a SARS-CoV-2 ORF6 expression plasmid with or without the expression plasmids for FLAG-RAE1 and HA-NUP98 and infected with SeV as described in the STAR Methods.

(J) Representative figures. Scale bars, 20 μm.

(K) Quantification of the subcellular localization of IRF3. GFP-positive cells (i.e., transfected cells) were classified based on subcellular localization of IRF3 (nucleus, cytosol, or both), and the proportion of each cell was calculated. The numbers above the bars indicate the numbers of counted cells.

(L and M) Effect of RAE1 and NUP98 overexpression on anti-IFN activity of ORF6. HEK293 cells were cotransfected with plasmids expressing SARS-CoV-2 ORF6 and p125Luc and three different amounts of plasmids expressing FLAG-tagged RAE1 and HA-tagged NUP98. 24 h after transfection, cells were infected with SeV (MOI 10). 24 h after infection, cells were harvested for a luciferase assay (L) and western blotting (M).

(legend continued on next page)

IFN induction, or IFN signaling (Figure 3L) in the presence of ORF6. Instead, western blotting revealed that overexpression of RAE1 and NUP98 increased the expression level of ORF6 in a dose-dependent manner (Figure 3M). Our findings suggest that ORF6 binds to RAE1 and NUP98 via its C-terminal region. However, overexpression of RAE1 and NUP98 cannot overcome the anti-IFN activity of ORF6.

SARS-CoV-2 variants that lost a functional *ORF6* gene have emerged during the current pandemic

Finally, we assessed the diversity and evolution of SARS-CoV-2 *ORF6* during the current pandemic. We downloaded 67,136 viral genome sequences from the global initiative on sharing all influenza data (GISAID) database (https://www.gisaid.org; as of July 16, 2020) and removed 395 sequences containing undetermined and/or mixed nucleotides in the *ORF6* region. By analyzing the *ORF6* region, we found that approximately 0.2% (124 of 66,741) sequences of pandemic viruses lost their C-terminal region because of frameshift and/or nonsense mutations (Figure 4A; Table S2). A SARS-CoV-2 variant encoding truncated ORF6 was first isolated in China on February 8, 2020 (GISAID: EPI_ISL_451350) (Figure 4A). We assessed the frequency of SARS-CoV-2 variants encoding truncated ORF6 for each country but found no specific deviations of the emergence of the ORF6-truncated SARS-CoV-2 at the country level (Table S3).

Based on the classification into pangolin lineages (https://github.com/cov-lineages/pangolin) and GISAID clades (Table S4), we then assessed how often ORF6-truncated SARS-CoV-2 variants have emerged during the current pandemic. We identified 54 separate clusters, strongly suggesting that at least 54 mutations shortening the coding sequence of *ORF6* emerged independently during the current pandemic (Table S4). To investigate whether ORF6-truncated SARS-CoV-2 variants have also spread via human-to-human transmission during the current pandemic, we analyzed cluster 41, which comprises 13 ORF6-truncated SARS-CoV-2 sequences in more detail. Twelve of the 13 ORF6-truncated SARS-CoV-2 genomes in cluster 41 were isolated in Wales, United Kingdom, and classified into pangolin lineage B.1.5 and GISAID clade G (Table S4). We then obtained 137 SARS-CoV-2 genome sequences that meet the abovementioned criteria (isolated in Wales, United Kingdom; pangolin lineage B.1.5 and GISAID clade G), including the 12 sequences belonging to cluster 41, and conducted a phylogenetic analysis. As shown in Figure 4B, 11 of the 12 ORF6-truncated SARS-CoV-2 mutants in cluster 41 formed a single clade. This observation suggests that these ORF6-truncated SARS-CoV-2 mutants have sporadically spread via human-to-human transmission. Together with our findings that deletion of the C-terminal region of SARS-CoV-2 ORF6 abolishes its ability to suppress IFN responses (Figure 3H), our analyses suggest that SARS-CoV-2 variants that lost a functional *ORF6* gene have emerged during the current COVID-19 pandemic and have the capacity to spread in the human population.

DISCUSSION

Here we provide evidence suggesting that SARS-CoV-2 ORF6 inhibits induction of human innate immune signaling, including induction of *IFNB1* and *IFNL1* as well as upregulation of ISGs triggered by IFN-I and IFN-III. During the review process of this paper, several recent publications have described mechanisms of IFN-I antagonism by different SARS-CoV-2 proteins, including ORF6 (Lei et al., 2020; Li et al., 2020a; Miorin et al., 2020; Xia et al., 2020; Yuen et al., 2020). Nevertheless, several findings of our work clearly set our study apart from previous work. We found that (1) the *ORF6* gene is specific to sarbecoviruses (Figure 1C); (2) not only the ORF6 proteins of human sarbecoviruses (i.e., SARS-CoV-2 and SARS-CoV) but also those of non-human sarbecoviruses from bats and a pangolin exert anti-IFN activity (Figure 2C); (3) the anti-IFN activity of ORF6 proteins of the SARS-CoV-2 lineage is higher than that of the SARS-CoV lineage (Figure 2C); (4) two residues, E46 and Q56, determine the anti-IFN activity of ORF6 (Figures 3A–3E, S2B, and S2C); (5) the anti-IFN activity of SARS-CoV-2 ORF6 completely depends on its C-terminal region whereas that of SARS-CoV ORF6 does not (Figures 3F–3H and S2D); (6) although previous papers suggested that ivermectin (Caly et al., 2020) and/or selinexor (Gordon et al., 2020) target ORF6, these compounds do not affect the anti-IFN activity of ORF6 (Figure S1A); and (7) SARS-CoV-2 mutants with truncations of the *ORF6* gene emerged during the current pandemic and most likely spread in the human population (Figure 4).

The observation that ORF6 proteins from SARS-CoV-2 and related viruses in bats and pangolins are, on average, more active in suppressing IFN responses than their SARS-CoV counterparts is reminiscent of the recently identified IFN antagonist ORF3b. This protein is also more potent in viruses of the SARS-CoV-2 lineage than in SARS-CoV and related animal viruses (Konno et al., 2020). These findings suggest that multiple IFN antagonists, including ORF6 and ORF3b, can cooperatively contribute to the inefficient and delayed IFN-I/III responses in SARS-CoV-2-infected cells as well as individuals with COVID-19 (Blanco-Melo et al., 2020; Hadjadj et al., 2020).

Consistent with previous studies characterizing ORF6 of SARS-CoV-2 (Miorin et al., 2020) or SARS-CoV (Kopecky-Bromberg et al., 2007), we show that SARS-CoV-2 ORF6 inhibits nuclear import of IRF3. Importantly, our mutational analyses revealed that inhibition of innate immune signaling by *Sarbecovirus* ORF6 proteins depends on their C-terminal region. Because *Sarbecovirus* ORF6 proteins bind RAE1 and NUP98 via their C-terminal region (Figure 3I), it has been suggested that ORF6 inhibits innate immune signaling by targeting these two host factors (Miorin et al., 2020). In contrast to this recent study

For western blotting (B, D, G, I, and M), the input of cell lysate was normalized to TUBA, and one representative result out of three independent experiments is shown. For the luciferase assay (C, E, H, and L), the value was normalized to unstimulated, empty vector-transfected cells (no SeV infection). In (C), statistically significant differences ($p < 0.05$) compared with SARS-CoV-2 (Wuhan-Hu-1) ORF6 WT-transfected cells (*) are shown. In (E), statistically significant differences ($p < 0.05$) compared with SARS-CoV (Tor2) ORF6 WT-transfected cells (*) are shown.
See also Figure S2.

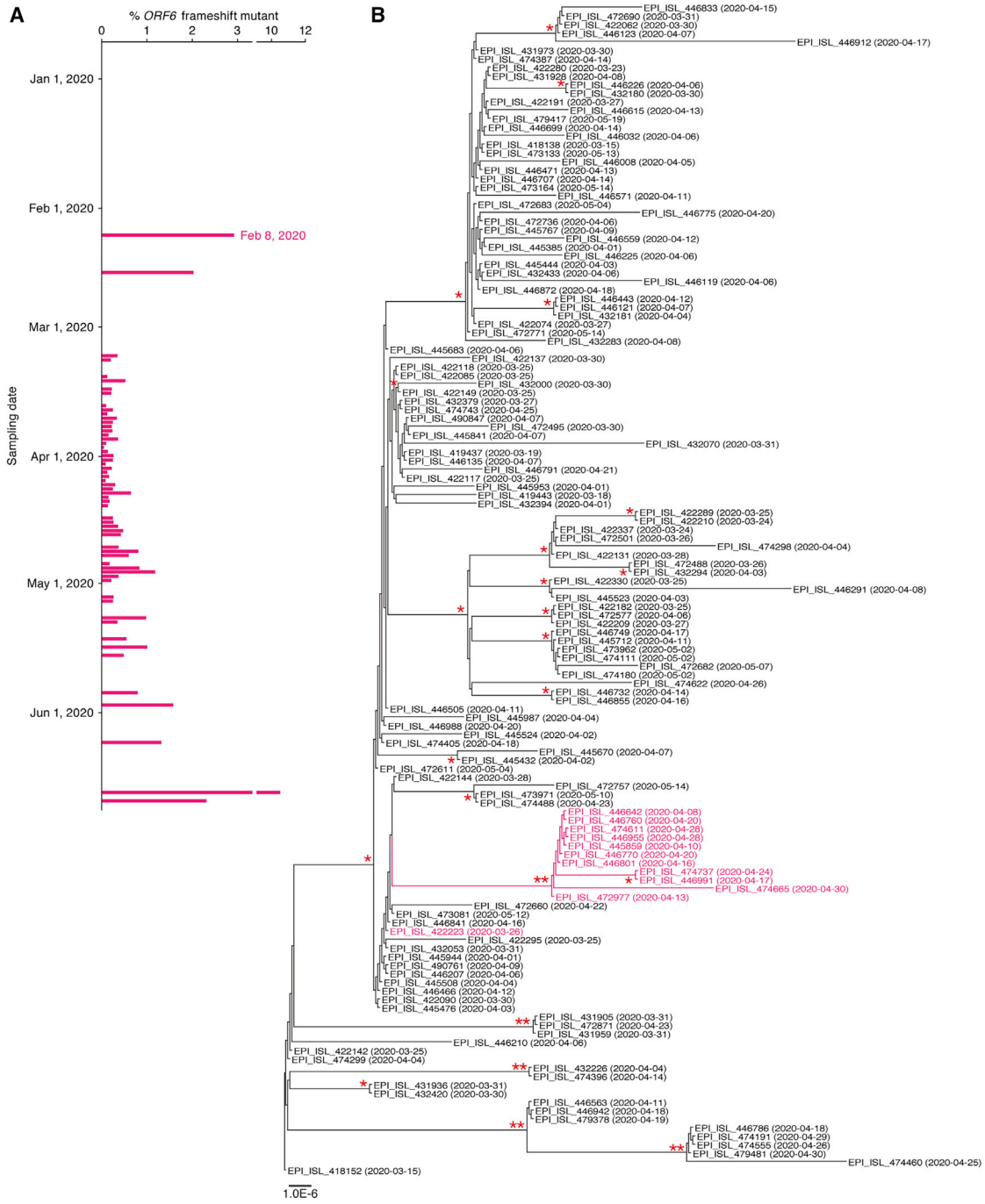

Figure 4. Emergence of ORF6-truncated SARS-CoV-2 mutants during the current pandemic

(A) Emergence of SARS-CoV-2 variants encoding truncated ORF6 during the current pandemic. The percentage of isolates encoding truncated ORF6 is shown for each day. A virus encoding truncated ORF6 was first detected on February 8, 2020 in China (GISAID: EPI_ISL_451350). Additional information is provided in Tables S2, S3, and S4.

(B) A maximum likelihood phylogenetic tree of the 137 SARS-CoV-2 genomes containing cluster 41. The tree was generated using the 137 SARS-CoV-2 genomes isolated in Wales, United Kingdom, and classified into pangolin lineage B.1.5 and GISAID clade G. The tree contains cluster 41 (pink), which is comprised of the 12 SARS-CoV-2 genomes with C-terminally truncated ORF6. The ORF6 sequence in cluster 41 is shown in Figure S3. GISAID ID and sampling date (in parentheses) are noted in each node. Bootstrap values; **, > 85%; *, > 60%.

See also Figure S3 and Tables S2, S3, and S4.

(Miorin et al., 2020), however, overexpression of RAE1 and NUP98 did not rescue the IFN response in the presence of ORF6 in our hands. Intriguingly, we found that the expression levels of ORF6 are increased upon expression of RAE1 and NUP98 (Figure 3M). Although RAE1 exports RNA from the nucleus, NUP98 is a component of the nuclear pore complex (Pritchard et al., 1999; Ren et al., 2010). Thus, overexpression of RAE1 and NUP98 may exert two opposing effects on ORF6-mediated IFN inhibition. On one hand, their overexpression may enhance IFN responses by compensating for RAE1/NUP98 proteins targeted by ORF6. On the other hand, RAE1/NUP98 may suppress IFN responses by increasing export of *ORF6* mRNA and, hence, total ORF6 protein levels. Our experiments suggest that these two effects may potentially annul each other.

In contrast to SARS-CoV-2 ORF6, the C-terminally truncated mutants of the ORF6 proteins of SARS-CoV lineages and two outgroup viruses (BtKY72 and BM48) only partially lost their ability to suppress induction of IFN activation. These observations suggest that *Sarbecovirus* ORF6 proteins other than those of SARS-CoV-2 can exert anti-IFN activity independent of their C-terminal region. This inhibitory activity most likely involves a mechanism that is independent of RAE1/NUP98 because recruitment of these proteins depends on the C terminus of ORF6. Notably, Xia et al. (2020) recently demonstrated that SARS-CoV-2 ORF6 antagonizes IRF3 nuclear import via targeting KPNA2, a subunit of importin, inhibiting type I IFN induction. Thus, it might be plausible to assume that SARS-CoV-2 ORF6 has evolved several independent mechanisms to counteract IFN-mediated immune responses, only some of which involve the C terminus of ORF6.

Incidentally, in the Dox-inducible ORF6 expression system in A549 cells, differences in the ability of SARS-CoV-2 ORF6 and SARS-CoV ORF6 to suppress upregulation of *IFNB1* seemed to disappear (Figure 2G). Differences between HEK293 cells and A549 cells may be explained by at least two possibilities. First, the expression levels of ORF6 upon Dox stimulation in A549 cells are lower than those achieved by transient transfection of HEK293 cells (Figure S1B). Second, induction of *IFNB1* by SeV infection in A549 cells (~1,500-fold) is dramatically higher than in HEK293 cells (~50- to 100-fold) (Figures 2D and 2G). Thus, the relative antagonistic activity of ORF6 may be lower in A549 cells compared with HEK293 cells.

By analyzing more than 67,000 SARS-CoV-2 sequences, we found that variants lacking the C-terminal region of ORF6 because of frameshift and/or nonsense mutations emerged more than 50 times during the current COVID-19 pandemic (Figure 4; Table S4). In contrast, truncated *ORF6* genes have so far not been detected in SARS-CoV-2-related viruses isolated from animals. By analyzing the *ORF6* sequences from a variety of sarbecoviruses belonging to the SARS-CoV lineage, however, we also found three SARS-CoV-related viruses isolated from two bats (GenBank: MK211374 and KJ473816) and a palm civet (GenBank: FJ959407) harboring truncated ORF6 sequences (44, 50, and 44 amino acids, respectively) because of frameshift mutations (Figure S3). Furthermore, we detected a human SARS-CoV, strain TWJ (GenBank: AP006558) that encodes a shortened ORF6 protein because of a frameshift mutation (Figure S3). Considering phylogenetic relationships and their mutation patterns, these ORF6 mutations emerged independently because the respective viruses do not form a single clade (Nakagawa and Miyazawa, 2020). These results suggest that truncations of ORF6 occurred multiple times in the subgenus *Sarbecovirus*, although such mutations have not spread dominantly in the viral population.

Because the C-terminal region of SARS-CoV-2 ORF6 is essential to elicit its anti-IFN activity, SARS-CoV-2 variants expressing C-terminally truncated ORF6 most likely lost an IFN antagonist. Although the frequency of SARS-CoV-2 isolates with C-terminally truncated ORF6 is low (~0.2%), our phylogenetic analyses provide strong evidence of human-to-human transmission of these viruses (Figure 4B). Because ORF6 is a potent IFN antagonist, the emergence of SARS-CoV-2 *ORF6* frameshift mutants may contribute to attenuation of viral pathogenicity. However, the relative contribution of ORF6 to disease severity is hard to assess at this point because most of the viral sequences currently deposited in GISAID are derived from symptomatic individuals (mostly severe cases). Thus, monitoring the *ORF6* gene during the current pandemic, not only in symptomatic individuals but also in asymptomatic carriers, and possible associations with viral pathogenicity seem to be highly warranted.

A limitation of this study is that the biological activity of *Sarbecovirus* ORF6 was investigated using an overexpression system. Additionally, all previous studies characterizing the anti-innate immune activity of ORF6 (Lei et al., 2020; Li et al., 2020a; Miorin et al., 2020; Xia et al., 2020; Yuen et al., 2020) have exclusively used overexpression systems, mainly in HEK293 cells. To fully define the relative contribution of ORF6 to immune evasion of SARS-CoV-2 and its effects on viral replication and pathogenicity, use of infectious, gene-modified recombinant viruses, preferentially in primary target cells, will be required. A variety of techniques to artificially reconstruct infectious SARS-CoV-2 by reverse genetics have been established (Rihn et al., 2021; Thi Nhu Thao et al., 2020; Torii et al., 2020; Xie et al., 2020, 2021; Ye et al., 2020). Future investigation using the recombinant SARS-CoV-2, in which *ORF6* gene is artificially modified, will unveil the biological activity of ORF6 to immune evasion of SARS-CoV-2.

STAR★METHODS

Detailed methods are provided in the online version of this paper and include the following:

- KEY RESOURCES TABLE
- RESOURCE AVAILABILITY
  - Lead contact
  - Materials availability
  - Data and code availability
- EXPERIMENTAL MODEL AND SUBJECT DETAILS
  - Cell Culture
- METHOD DETAILS
  - Viral Genomes and Phylogenetic Analyses
  - Plasmid Construction
  - Transfection, Dox Treatment, IFN treatment and SeV Infection

- Reporter Assay
- Western Blotting
- Co-IP
- Real-time RT-PCR
- Immunofluorescence Staining
- SARS-CoV-2 Sequence Analysis

● QUANTIFICATION AND STATISTICAL ANALYSIS

SUPPLEMENTAL INFORMATION

Supplemental information can be found online at https://doi.org/10.1016/j.celrep.2021.108916.

ACKNOWLEDGMENTS

We would like to thank all laboratory members in the Division of Systems Virology, Institute of Medical Science, The University of Tokyo, Japan and all authors who have kindly deposited and shared genome data on GISAID. We also thank Naoko Misawa (Institute for Life and Medical Sciences, Kyoto University, Japan), Robert J. Gifford and David L. Robertson (MRC-University of Glasgow Centre for Virus Research, United Kingdom), and Takashi Irie (Hiroshima University, Japan) for generous support; Takashi Fujita (Institute for Life and Medical Sciences, Kyoto University, Japan) for providing p125Luc; Yoshio Koyanagi (Institute for Life and Medical Sciences, Kyoto University, Japan) for providing the HA-tagged NUP98 expression plasmid; Karl-Klaus Conzelmann (Ludwig Maximilians University, Germany) for providing pISRE-Luc; and Nevan J. Krogan (University of California, San Francisco, CA, USA) for providing the pLVX-TetOne-Puro plasmid expressing GFP. We thank Kotubu Misawa for dedicated support. The super-computing resource SHIROKANE was provided by the Human Genome Center, Institute of Medical Science, The University of Tokyo, Japan. This study was supported in part by AMED Research Program on Emerging and Re-emerging Infectious Diseases 20fk0108146 (to K.S.), 19fk0108171 (to S.N. and K.S.), 20fk0108270 (to K.S.), and 20fk0108413 (to S.N. and K.S.); AMED Research Program on HIV/AIDS 19fk0410019 and 20fk0410014 (to K.S.); JST J-RAPID JPMJJR2007 (to K.S.); JST SICORP (e-ASIA) JPMJSC20U1 (to K.S.); JST CREST JPMJCR20H6 (to S.N.) and JPMJCR20H4 (to K.S.); JSPS KAKENHI Grant-in-Aid for Scientific Research B 18H02662 (to K.S.); JSPS KAKENHI Grants-in-Aid for Scientific Research on Innovative Areas 16H06429 and 16K21723 (to S.N. and K.S.), 17H05823 and 19H04843 (to S.N.), and 17H05813 and 19H04826 (to K.S.); JSPS Fund for the Promotion of Joint International Research (Fostering Joint International Research) 18KK0447 (to K.S.); JSPS Research Fellowships DC1 19J20488 (to I.K.) and DC1 19J22914 (to Y.K.); the ONO Medical Research Foundation (to K.S.); the Ichiro Kanehara Foundation (to K.S.); the Lotte Foundation (to K.S.); the Mochida Memorial Foundation for Medical and Pharmaceutical Research (to K.S.); the Daiichi Sankyo Foundation of Life Science (to K.S.); the Sumitomo Foundation (to K.S.); the Uehara Foundation (to K.S.); the Takeda Science Foundation (to K.S.); the Tokyo Biochemical Research Foundation (to K.S.); the JSPS Core-to-Core Program (A. Advanced Research Networks) (to K.S.); the Canon Foundation in Europe (to D.S. and K.S.); the International Graduate School in Molecular Medicine Ulm (IGradU) (to K.H.); a COVID-19 research grant of the Federal Ministry of Education and Research (MWK) Baden-Württemberg (to D.S.); the Heisenberg Program of the German Research Foundation (to D.S.); 2020 Tokai University School of Medicine research aid (to S.N.); and the International Joint Research Project of the Institute of Medical Science, The University of Tokyo 2020-K3003 (to D.S. and K.S.).

AUTHOR CONTRIBUTIONS

I.K., Y.K., K.U., and K.H. performed the experiments. S.N. performed the molecular phylogenetic analysis. I.K., Y.K., K.U., K.H., D.S., and K.S. interpreted the results. D.S. and K.S. designed the experiments. D.S. and K.S. wrote the manuscript. All authors reviewed and proofread the manuscript.

Received: September 2, 2020
Revised: January 24, 2021
Accepted: March 8, 2021
Published: March 30, 2021

REFERENCES

Blanco-Melo, D., Nilsson-Payant, B.E., Liu, W.-C., Uhl, S., Hoagland, D., Møller, R., Jordan, T.X., Oishi, K., Panis, M., Sachs, D., et al. (2020). Imbalanced host response to SARS-CoV-2 drives development of COVID-19. Cell *181*, 1036–1045.e9.

Boni, M.F., Lemey, P., Jiang, X., Lam, T.T., Perry, B.W., Castoe, T.A., Rambaut, A., and Robertson, D.L. (2020). Evolutionary origins of the SARS-CoV-2 sarbecovirus lineage responsible for the COVID-19 pandemic. Nat. Microbiol. *5*, 1408–1417.

Brzózka, K., Finke, S., and Conzelmann, K.K. (2006). Inhibition of interferon signaling by rabies virus phosphoprotein P: activation-dependent binding of STAT1 and STAT2. J. Virol. *80*, 2675–2683.

Caly, L., Druce, J.D., Catton, M.G., Jans, D.A., and Wagstaff, K.M. (2020). The FDA-approved drug ivermectin inhibits the replication of SARS-CoV-2 in vitro. Antiviral Res. *178*, 104787.

Capella-Gutiérrez, S., Silla-Martínez, J.M., and Gabaldón, T. (2009). trimAl: a tool for automated alignment trimming in large-scale phylogenetic analyses. Bioinformatics *25*, 1972–1973.

Chan-Yeung, M., and Xu, R.H. (2003). SARS: epidemiology. Respirology *8* (*Suppl*), S9–S14.

Darriba, D., Posada, D., Kozlov, A.M., Stamatakis, A., Morel, B., and Flouri, T. (2020). ModelTest-NG: A new and scalable tool for the selection of DNA and protein evolutionary models. Mol. Biol. Evol. *37*, 291–294.

Ebina, H., Aoki, J., Hatta, S., Yoshida, T., and Koyanagi, Y. (2004). Role of Nup98 in nuclear entry of human immunodeficiency virus type 1 cDNA. Microbes Infect. *6*, 715–724.

Franks, T.M., McCloskey, A., Shokirev, M.N., Benner, C., Rathore, A., and Hetzer, M.W. (2017). Nup98 recruits the Wdr82-Set1A/COMPASS complex to promoters to regulate H3K4 trimethylation in hematopoietic progenitor cells. Genes Dev. *31*, 2222–2234.

Frieman, M., Yount, B., Heise, M., Kopecky-Bromberg, S.A., Palese, P., and Baric, R.S. (2007). Severe acute respiratory syndrome coronavirus ORF6 antagonizes STAT1 function by sequestering nuclear import factors on the rough endoplasmic reticulum/Golgi membrane. J. Virol. *81*, 9812–9824.

Fujita, T., Nolan, G.P., Liou, H.C., Scott, M.L., and Baltimore, D. (1993). The candidate proto-oncogene bcl-3 encodes a transcriptional coactivator that activates through NF-kappa B p50 homodimers. Genes Dev. *7* (*7B*), 1354–1363.

García-Sastre, A., Egorov, A., Matassov, D., Brandt, S., Levy, D.E., Durbin, J.E., Palese, P., and Muster, T. (1998). Influenza A virus lacking the NS1 gene replicates in interferon-deficient systems. Virology *252*, 324–330.

Ge, X.Y., Li, J.L., Yang, X.L., Chmura, A.A., Zhu, G., Epstein, J.H., Mazet, J.K., Hu, B., Zhang, W., Peng, C., et al. (2013). Isolation and characterization of a bat SARS-like coronavirus that uses the ACE2 receptor. Nature *503*, 535–538.

Gordon, D.E., Jang, G.M., Bouhaddou, M., Xu, J., Obernier, K., White, K.M., O'Meara, M.J., Rezelj, V.V., Guo, J.Z., Swaney, D.L., et al. (2020). A SARS-CoV-2 protein interaction map reveals targets for drug repurposing. Nature *583*, 459–468.

Hadjadj, J., Yatim, N., Barnabei, L., Corneau, A., Boussier, J., Smith, N., Péré, H., Charbit, B., Bondet, V., Chenevier-Gobeaux, C., et al. (2020). Impaired type I interferon activity and inflammatory responses in severe COVID-19 patients. Science *369*, 718–724.

Hayn, M., Hirschenberger, M., Koepke, L., Straub, J.H., Nchioua, R., Christensen, M.H., Klute, S., Bozzo, C.P., Aftab, W., Zech, F., et al. (2020). Imperfect innate immune antagonism renders SARS-CoV-2 vulnerable towards IFN-γ and -λ. bioRxiv. https://doi.org/10.1101/2020.10.15.340612.

He, B., Zhang, Y., Xu, L., Yang, W., Yang, F., Feng, Y., Xia, L., Zhou, J., Zhen, W., Feng, Y., et al. (2014). Identification of diverse alphacoronaviruses and genomic characterization of a novel severe acute respiratory syndrome-like coronavirus from bats in China. J. Virol. *88*, 7070–7082.

Hu, B., Zeng, L.P., Yang, X.L., Ge, X.Y., Zhang, W., Li, B., Xie, J.Z., Shen, X.R., Zhang, Y.Z., Wang, N., et al. (2017). Discovery of a rich gene pool of bat SARS-related coronaviruses provides new insights into the origin of SARS coronavirus. PLoS Pathog. *13*, e1006698.

Katoh, K., and Standley, D.M. (2013). MAFFT multiple sequence alignment software version 7: improvements in performance and usability. Mol. Biol. Evol. *30*, 772–780.

Kobayashi, T., Takeuchi, J.S., Ren, F., Matsuda, K., Sato, K., Kimura, Y., Misawa, N., Yoshikawa, R., Nakano, Y., Yamada, E., et al. (2014). Characterization of red-capped mangabey tetherin: implication for the co-evolution of primates and their lentiviruses. Sci. Rep. *4*, 5529.

Kochs, G., García-Sastre, A., and Martínez-Sobrido, L. (2007). Multiple anti-interferon actions of the influenza A virus NS1 protein. J. Virol. *81*, 7011–7021.

Konno, Y., Nagaoka, S., Kimura, I., Takahashi Ueda, M., Kumata, R., Ito, J., Nakagawa, S., Kobayashi, T., Koyanagi, Y., and Sato, K. (2018). A naturally occurring feline APOBEC3 variant that loses anti-lentiviral activity by lacking two amino acid residues. J. Gen. Virol. *99*, 704–709.

Konno, Y., Kimura, I., Uriu, K., Fukushi, M., Irie, T., Koyanagi, Y., Sauter, D., Gifford, R.J., Nakagawa, S., and Sato, K.; USFQ-COVID19 Consortium (2020). SARS-CoV-2 ORF3b is a potent interferon antagonist whose activity is increased by a naturally occurring elongation variant. Cell Rep. *32*, 108185.

Kopecky-Bromberg, S.A., Martínez-Sobrido, L., Frieman, M., Baric, R.A., and Palese, P. (2007). Severe acute respiratory syndrome coronavirus open reading frame (ORF) 3b, ORF 6, and nucleocapsid proteins function as interferon antagonists. J. Virol. *81*, 548–557.

Kozlov, A.M., Darriba, D., Flouri, T., Morel, B., and Stamatakis, A. (2019). RAxML-NG: a fast, scalable and user-friendly tool for maximum likelihood phylogenetic inference. Bioinformatics *35*, 4453–4455.

Krug, R.M., Yuan, W., Noah, D.L., and Latham, A.G. (2003). Intracellular warfare between human influenza viruses and human cells: the roles of the viral NS1 protein. Virology *309*, 181–189.

Lai, M.M., Brayton, P.R., Armen, R.C., Patton, C.D., Pugh, C., and Stohlman, S.A. (1981). Mouse hepatitis virus A59: mRNA structure and genetic localization of the sequence divergence from hepatotropic strain MHV-3. J. Virol. *39*, 823–834.

Lam, T.T., Jia, N., Zhang, Y.W., Shum, M.H., Jiang, J.F., Zhu, H.C., Tong, Y.G., Shi, Y.X., Ni, X.B., Liao, Y.S., et al. (2020). Identifying SARS-CoV-2-related coronaviruses in Malayan pangolins. Nature *583*, 282–285.

Langer, S., Hammer, C., Hopfensperger, K., Klein, L., Hotter, D., De Jesus, P.D., Herbert, K.M., Pache, L., Smith, N., van der Merwe, J.A., et al. (2019). HIV-1 Vpu is a potent transcriptional suppressor of NF-κB-elicited antiviral immune responses. eLife *8*, e41930.

Lau, S.K., Woo, P.C., Li, K.S., Huang, Y., Tsoi, H.W., Wong, B.H., Wong, S.S., Leung, S.Y., Chan, K.H., and Yuen, K.Y. (2005). Severe acute respiratory syndrome coronavirus-like virus in Chinese horseshoe bats. Proc. Natl. Acad. Sci. USA *102*, 14040–14045.

Lau, S.K., Li, K.S., Huang, Y., Shek, C.T., Tse, H., Wang, M., Choi, G.K., Xu, H., Lam, C.S., Guo, R., et al. (2010). Ecoepidemiology and complete genome comparison of different strains of severe acute respiratory syndrome-related Rhinolophus bat coronavirus in China reveal bats as a reservoir for acute, self-limiting infection that allows recombination events. J. Virol. *84*, 2808–2819.

Lei, X., Dong, X., Ma, R., Wang, W., Xiao, X., Tian, Z., Wang, C., Wang, Y., Li, L., Ren, L., et al. (2020). Activation and evasion of type I interferon responses by SARS-CoV-2. Nat. Commun. *11*, 3810.

Li, W., Shi, Z., Yu, M., Ren, W., Smith, C., Epstein, J.H., Wang, H., Crameri, G., Hu, Z., Zhang, H., et al. (2005). Bats are natural reservoirs of SARS-like coronaviruses. Science *310*, 676–679.

Li, J.Y., Liao, C.H., Wang, Q., Tan, Y.J., Luo, R., Qiu, Y., and Ge, X.Y. (2020a). The ORF6, ORF8 and nucleocapsid proteins of SARS-CoV-2 inhibit type I interferon signaling pathway. Virus Res. *286*, 198074.

Li, X., Giorgi, E.E., Marichannegowda, M.H., Foley, B., Xiao, C., Kong, X.-P., Chen, Y., Gnanakaran, S., Korber, B., and Gao, F. (2020b). Emergence of SARS-CoV-2 through recombination and strong purifying selection. Sci. Adv. *6*, eabb9153.

Lin, X.D., Wang, W., Hao, Z.Y., Wang, Z.X., Guo, W.P., Guan, X.Q., Wang, M.R., Wang, H.W., Zhou, R.H., Li, M.H., et al. (2017). Extensive diversity of coronaviruses in bats from China. Virology *507*, 1–10.

McIntosh, K., Becker, W.B., and Chanock, R.M. (1967). Growth in suckling-mouse brain of "IBV-like" viruses from patients with upper respiratory tract disease. Proc. Natl. Acad. Sci. USA *58*, 2268–2273.

Miorin, L., Kehrer, T., Sanchez-Aparicio, M.T., Zhang, K., Cohen, P., Patel, R.S., Cupic, A., Makio, T., Mei, M., Moreno, E., et al. (2020). SARS-CoV-2 Orf6 hijacks Nup98 to block STAT nuclear import and antagonize interferon signaling. Proc. Natl. Acad. Sci. USA *117*, 28344–28354.

Nakagawa, S., and Miyazawa, T. (2020). Genome evolution of SARS-CoV-2 and its virological characteristics. Inflamm. Regen. *40*, 17.

Nakano, Y., Misawa, N., Juarez-Fernandez, G., Moriwaki, M., Nakaoka, S., Funo, T., Yamada, E., Soper, A., Yoshikawa, R., Ebrahimi, D., et al. (2017). HIV-1 competition experiments in humanized mice show that APOBEC3H imposes selective pressure and promotes virus adaptation. PLoS Pathog. *13*, e1006348.

Niwa, H., Yamamura, K., and Miyazaki, J. (1991). Efficient selection for high-expression transfectants with a novel eukaryotic vector. Gene *108*, 193–199.

Perlman, S., and Masters, P.S. (2020). *Coronaviridae*: the viruses and their replication. In Fields Virology, D.M. Knipe and P.M. Howley, eds. (Lippincott Williams & Wilkins), pp. 410–448.

Pritchard, C.E., Fornerod, M., Kasper, L.H., and van Deursen, J.M. (1999). RAE1 is a shuttling mRNA export factor that binds to a GLEBS-like NUP98 motif at the nuclear pore complex through multiple domains. J. Cell Biol. *145*, 237–254.

Quan, P.L., Firth, C., Street, C., Henriquez, J.A., Petrosov, A., Tashmukhamedova, A., Hutchison, S.K., Egholm, M., Osinubi, M.O., Niezgoda, M., et al. (2010). Identification of a severe acute respiratory syndrome coronavirus-like virus in a leaf-nosed bat in Nigeria. MBio *1*, e00208.

Rambaut, A., Holmes, E.C., O'Toole, Á., Hill, V., McCrone, J.T., Ruis, C., du Plessis, L., and Pybus, O.G. (2020). A dynamic nomenclature proposal for SARS-CoV-2 lineages to assist genomic epidemiology. Nat. Microbiol. *5*, 1403–1407.

Ren, Y., Seo, H.S., Blobel, G., and Hoelz, A. (2010). Structural and functional analysis of the interaction between the nucleoporin Nup98 and the mRNA export factor Rae1. Proc. Natl. Acad. Sci. USA *107*, 10406–10411.

Rihn, S.J., Merits, A., Bakshi, S., Turnbull, M.L., Wickenhagen, A., Alexander, A.J.T., Baillie, C., Brennan, B., Brown, F., Brunker, K., et al. (2021). A plasmid DNA-launched SARS-CoV-2 reverse genetics system and coronavirus toolkit for COVID-19 research. PLoS Biol. *19*, e3001091.

Spaan, W., Cavanagh, D., and Horzinek, M.C. (1988). Coronaviruses: structure and genome expression. J. Gen. Virol. *69*, 2939–2952.

Tang, X.C., Zhang, J.X., Zhang, S.Y., Wang, P., Fan, X.H., Li, L.F., Li, G., Dong, B.Q., Liu, W., Cheung, C.L., et al. (2006). Prevalence and genetic diversity of coronaviruses in bats from China. J. Virol. *80*, 7481–7490.

Thi Nhu Thao, T., Labroussaa, F., Ebert, N., V'kovski, P., Stalder, H., Portmann, J., Kelly, J., Steiner, S., Holwerda, M., Kratzel, A., et al. (2020). Rapid reconstruction of SARS-CoV-2 using a synthetic genomics platform. Nature *582*, 561–565.

Torii, S., Ono, C., Suzuki, R., Morioka, Y., Anzai, I., Fauzyah, Y., Maeda, Y., Kamitani, W., Fukuhara, T., and Matsuura, Y. (2020). Establishment of a reverse genetics system for SARS-CoV-2 using circular polymerase extension reaction. bioRxiv. https://doi.org/10.1101/2020.09.23.309849.

Ueda, M.T., Kurosaki, Y., Izumi, T., Nakano, Y., Oloniniyi, O.K., Yasuda, J., Koyanagi, Y., Sato, K., and Nakagawa, S. (2017). Functional mutations in spike

glycoprotein of Zaire ebolavirus associated with an increase in infection efficiency. Genes Cells *22*, 148–159.

van Boheemen, S., de Graaf, M., Lauber, C., Bestebroer, T.M., Raj, V.S., Zaki, A.M., Osterhaus, A.D., Haagmans, B.L., Gorbalenya, A.E., Snijder, E.J., and Fouchier, R.A. (2012). Genomic characterization of a newly discovered coronavirus associated with acute respiratory distress syndrome in humans. MBio *3*, e00473-12.

Wang, M., Yan, M., Xu, H., Liang, W., Kan, B., Zheng, B., Chen, H., Zheng, H., Xu, Y., Zhang, E., et al. (2005). SARS-CoV infection in a restaurant from palm civet. Emerg. Infect. Dis. *11*, 1860–1865.

Wang, L., Fu, S., Cao, Y., Zhang, H., Feng, Y., Yang, W., Nie, K., Ma, X., and Liang, G. (2017). Discovery and genetic analysis of novel coronaviruses in least horseshoe bats in southwestern China. Emerg. Microbes Infect. *6*, e14.

Weiss, S.R. (2020). Forty years with coronaviruses. J. Exp. Med. *217*, e20200537.

WHO (2004). Summary of probable SARS cases with onset of illness from 1 November 2002 to 31 July 2003. https://www.who.int/publications/m/item/summary-of-probable-sars-cases-with-onset-of-illness-from-1-november-2002-to-31-july-2003.

WHO (2019). Middle East respiratory syndrome coronavirus (MERS-CoV). https://www.who.int/health-topics/middle-east-respiratory-syndrome-coronavirus-mers.

WHO (2020). Coronavirus disease 2019. https://www.who.int/emergencies/diseases/novel-coronavirus-2019.

Woo, P.C., Lau, S.K., Chu, C.M., Chan, K.H., Tsoi, H.W., Huang, Y., Wong, B.H., Poon, R.W., Cai, J.J., Luk, W.K., et al. (2005). Characterization and complete genome sequence of a novel coronavirus, coronavirus HKU1, from patients with pneumonia. J. Virol. *79*, 884–895.

Woo, P.C., Wang, M., Lau, S.K., Xu, H., Poon, R.W., Guo, R., Wong, B.H., Gao, K., Tsoi, H.W., Huang, Y., et al. (2007). Comparative analysis of twelve genomes of three novel group 2c and group 2d coronaviruses reveals unique group and subgroup features. J. Virol. *81*, 1574–1585.

Wu, Z., Yang, L., Ren, X., He, G., Zhang, J., Yang, J., Qian, Z., Dong, J., Sun, L., Zhu, Y., et al. (2016a). Deciphering the bat virome catalog to better understand the ecological diversity of bat viruses and the bat origin of emerging infectious diseases. ISME J. *10*, 609–620.

Wu, Z., Yang, L., Ren, X., Zhang, J., Yang, F., Zhang, S., and Jin, Q. (2016b). ORF8-related genetic evidence for Chinese horseshoe bats as the source of human severe acute respiratory syndrome coronavirus. J. Infect. Dis. *213*, 579–583.

Xia, H., Cao, Z., Xie, X., Zhang, X., Chen, J.Y., Wang, H., Menachery, V.D., Rajsbaum, R., and Shi, P.Y. (2020). Evasion of type I interferon by SARS-CoV-2. Cell Rep. *33*, 108234.

Xiao, K., Zhai, J., Feng, Y., Zhou, N., Zhang, X., Zou, J.-J., Li, N., Guo, Y., Li, X., Shen, X., et al. (2020). Isolation of SARS-CoV-2-related coronavirus from Malayan pangolins. Nature *583*, 286–289.

Xie, X., Muruato, A., Lokugamage, K.G., Narayanan, K., Zhang, X., Zou, J., Liu, J., Schindewolf, C., Bopp, N.E., Aguilar, P.V., et al. (2020). An infectious cDNA clone of SARS-CoV-2. Cell Host Microbe *27*, 841–848.e3.

Xie, X., Lokugamage, K.G., Zhang, X., Vu, M.N., Muruato, A.E., Menachery, V.D., and Shi, P.Y. (2021). Engineering SARS-CoV-2 using a reverse genetic system. Nat. Protoc. Published online January 29, 2021. https://doi.org/10.1038/s41596-021-00491-8.

Yamada, E., Nakaoka, S., Klein, L., Reith, E., Langer, S., Hopfensperger, K., Iwami, S., Schreiber, G., Kirchhoff, F., Koyanagi, Y., et al. (2018). Human-specific adaptations in Vpu conferring anti-tetherin activity are critical for efficient early HIV-1 replication *in vivo*. Cell Host Microbe *23*, 110–120.e7.

Ye, C., Chiem, K., Park, J.G., Oladunni, F., Platt, R.N., 2nd, Anderson, T., Almazan, F., de la Torre, J.C., and Martinez-Sobrido, L. (2020). Rescue of SARS-CoV-2 from a single bacterial artificial chromosome. MBio *11*, e02168-20.

Yoshida, A., Kawabata, R., Honda, T., Sakai, K., Ami, Y., Sakaguchi, T., and Irie, T. (2018). A single amino acid substitution within the paramyxovirus Sendai virus nucleoprotein is a critical determinant for production of interferon-beta-inducing copyback-type defective interfering genomes. J. Virol. *92*, e02094.

Yoshikawa, R., Takeuchi, J.S., Yamada, E., Nakano, Y., Misawa, N., Kimura, Y., Ren, F., Miyazawa, T., Koyanagi, Y., and Sato, K. (2017). Feline immunodeficiency virus evolutionarily acquires two proteins, Vif and protease, capable of antagonizing feline APOBEC3. J. Virol. *91*, e00250-17.

Yuan, J., Hon, C.C., Li, Y., Wang, D., Xu, G., Zhang, H., Zhou, P., Poon, L.L., Lam, T.T., Leung, F.C., and Shi, Z. (2010). Intraspecies diversity of SARS-like coronaviruses in Rhinolophus sinicus and its implications for the origin of SARS coronaviruses in humans. J. Gen. Virol. *91*, 1058–1062.

Yuen, C.K., Lam, J.Y., Wong, W.M., Mak, L.F., Wang, X., Chu, H., Cai, J.P., Jin, D.Y., To, K.K., Chan, J.F., et al. (2020). SARS-CoV-2 nsp13, nsp14, nsp15 and orf6 function as potent interferon antagonists. Emerg. Microbes Infect. *9*, 1418–1428.

Zaki, A.M., van Boheemen, S., Bestebroer, T.M., Osterhaus, A.D., and Fouchier, R.A. (2012). Isolation of a novel coronavirus from a man with pneumonia in Saudi Arabia. N. Engl. J. Med. *367*, 1814–1820.

Zhou, H., Chen, X., Hu, T., Li, J., Song, H., Liu, Y., Wang, P., Liu, D., Yang, J., Holmes, E.C., et al. (2020a). A novel bat coronavirus closely related to SARS-CoV-2 contains natural insertions at the S1/S2 cleavage site of the spike protein. Curr. Biol. *30*, 2196–2203.e3.

Zhou, P., Yang, X.L., Wang, X.G., Hu, B., Zhang, L., Zhang, W., Si, H.R., Zhu, Y., Li, B., Huang, C.L., et al. (2020b). A pneumonia outbreak associated with a new coronavirus of probable bat origin. Nature *579*, 270–273.

STAR★METHODS

KEY RESOURCES TABLE

REAGENT or RESOURCE	SOURCE	IDENTIFIER
Antibodies		
HRP-conjugated anti-HA	Roche	Cat# 12013819001; RRID: AB_390918
HRP-conjugated anti-Flag	Sigma-Aldrich	Cat# A8592; RRID: AB_439702
Anti-SARS-CoV-2 ORF6	Abnova	Cat# PAB31757; RRID: N/A
Anti-RAE1	Abcam	Cat# ab124783; RRID: AB_10973530
Anti-NUP98	Cell Signaling Technology	Cat# 2598; RRID: AB_2267700
Anti-alpha-Tubulin (TUBA)	Sigma-Aldrich	Cat# T9026; RRID: AB_477593
HRP-conjugated anti-mouse IgG	Cell Signaling Technology	Cat# 7076; RRID: AB_330924
HRP-conjugated anti-rabbit IgG	Cell Signaling Technology	Cat# 7074S; RRID: AB_2099233
Anti-IRF3	Cell Signaling Technology	Cat# 11904T; RRID: N/A
Alexa Flour 647-conjugated anti-rabbit IgG	Thermo Fisher Scientific	Cat# 21244; RRID: AB_2535812
Bacterial and virus strains		
SeV (strain Cantell, clone cCdi)	Yoshida et al., 2018	GenBank AB855654
Chemicals, peptides, and recombinant proteins		
Dulbecco's modified Eagle's medium	Sigma-Aldrich	Cat# D6046-500ML
Ham's F-12K medium	Thermo Fisher Scientific	Cat# 21127022
Fetal calf serum	Sigma-Aldrich	Cat# 172012-500ML
Penicillin streptomycin	Sigma-Aldrich	Cat# P4333-100ML
L-glutamate	Thermo Fisher Scientific	Cat# 25030081
Puromycin	Invivogen	Cat# ant-pr-1
Doxycycline	Takara	Cat# 1311N
Recombinant IFN-α	PBL Assay Science	Cat# 11200-2
Recombinant IFN-λ3	R&D Systems	Cat# 5259-IL-025
Ivermectin	Merck	Cat# I8898-1G
Selinexor	Selleck Chemicals	Cat# S7252
PrimeSTAR GXL DNA polymerase	Takara	Cat# R050A
XhoI	Takara	Cat# 1094A
BglII	Takara	Cat# 1021A
EcoRI	Takara	Cat# 1040A
BamHI	Takara	Cat# 1010A
EcoRV	Takara	Cat# 1042A
NotI	Takara	Cat# 1166A
PEI Max	Polysciences	Cat# 24765-1
SuperScript III reverse transcriptase	Thermo Fisher Scientific	Cat# 18080085
RNase-Free DNase Set	QIAGEN	Cat# 79254
Power SYBR Green PCR Master Mix	Thermo Fisher Scientific	Cat# 4367659
Protease inhibitor cocktail	Roche	Cat# 11873580001
DAPI	Sigma Aldrich	Cat# D9542-1MG
Mowiol mounting medium	Cold Spring Harbor Protocols	N/A
Critical commercial assays		
PicaGene BrillianStar-LT luciferase assay system	Toyo-b-net	Cat# BLT1000
CellTiter-Glo 2.0 assay kit	Promega	Cat# G9241
QIAamp RNA blood mini kit	QIAGEN	Cat# 52304
Anti-HA magnetic beads	MBL	Cat# M132-11

(*Continued on next page*)

Continued

REAGENT or RESOURCE	SOURCE	IDENTIFIER
Experimental models: cell lines		
Human: HEK293 cells	ATCC	CRL-1573
Human: HEK293T cells	ATCC	CRL-3216
Human: A549 cells	ATCC	CCL-185
Oligonucleotides		
Primers for plasmid construction, see Table S5	This study	N/A
Random primer	Thermo Fisher Scientific	Cat# 48190011
GAPDH forward primer for real-time RT-PCR: ATGGGGAAGGTGAAGGTCG	Konno et al., 2020	N/A
GAPDH reverse primer for real-time RT-PCR: GGGTCATTGATGGCAACAATATC	Konno et al., 2020	N/A
IFNB1 forward primer for real-time RT-PCR: AAACTCATGAGCAGTCTGCA	Konno et al., 2020	N/A
IFNB1 reverse primer for real-time RT-PCR: AGAGGCACAGGCTAGGAGATC	Konno et al., 2020	N/A
IFNL1 forward primer for real-time RT-PCR: ACCCTGAGTCCACCTGACAC	This study	N/A
IFNL1 reverse primer for real-time RT-PCR: AGTAGGGCTCAGCGCATAAA	This study	N/A
IFI44L reverse primer for real-time RT-PCR: GTTTTATGGCCACCGTCAGT	Yamada et al., 2018	N/A
IFI44L reverse primer for real-time RT-PCR: CTGGACTTTCCAGACCCAAC	Yamada et al., 2018	N/A
BST2 forward primer for real-time RT-PCR: TCTCCTGCAACAAGAGCTGACC	OriGene	Cat# HP207665
BST2 reverse primer for real-time RT-PCR: TCTCTGCATCCAGGGAAGCCAT	OriGene	Cat# HP207665
PARP9 reverse primer for real-time RT-PCR: GGCAAAGAGGTCCAAGATGCTG	OriGene	Cat# HP215603
PARP9 reverse primer for real-time RT-PCR: GCCTCACACATCTCTTCCACGT	OriGene	Cat# HP215603
Recombinant DNA		
Plasmid: pCAGGS	Niwa et al., 1991	N/A
Plasmid: pcDNA3.1	ThermoFisher Scientific	Cat# V800-20
Sarbecovirus ORF6, see Figure 2A	This study	N/A
Sarbecovirus ORF3b	ADDIN EN.CITE (	N/A
IAV A/Puerto Rico/8/34 NS1	This study	GenBank accession number EF467817.1
Plasmid: p125Luc	Fujita et al., 1993	N/A
Plasmid: pISRE-Luc	Brzózka et al., 2006	N/A
Plasmid: pLVX-TetOne-Puro	Takara	Cat# 631849
Plasmid: pFlag-RAE1	This study	N/A
Plasmid: pHA-NUP98	Ebina et al., 2004	N/A
Software and algorithms		
FigTree	Andrew Rambaut	http://tree.bio.ed.ac.uk/software/figtree
Sequencher version 5.1	Gene Codes Corporation	N/A
Prism	GraphPad Software	https://www.graphpad.com/scientific-software/prism/
L-INS-i in the MAFFT version 7.453	Katoh and Standley, 2013	https://mafft.cbrc.jp/alignment/software/
trimal version 1.4	Capella-Gutiérrez et al., 2009	http://trimal.cgenomics.org
ModelTest-NG version 0.1.5	Darriba et al., 2020	https://github.com/ddarriba/modeltest

(*Continued on next page*)

Continued

REAGENT or RESOURCE	SOURCE	IDENTIFIER
RAxML-NG version 1.0.0	Kozlov et al., 2019	https://github.com/amkozlov/raxml-ng
ImageJ	Open Source	https://imagej.net/Welcome
Zen	Zeiss	https://www.zeiss.de/mikroskopie/produkte/mikroskopsoftware/zen.html
Other		
GISAID	Freunde von GISAID e.V.	https://www.gisaid.org
Pangolin	Rambaut et al., 2020	https://cov-lineages.org/pangolin.html

RESOURCE AVAILABILITY

Lead contact

Further information and requests for resources and reagents should be directed to and will be fulfilled by the lead contact, Kei Sato (KeiSato@g.ecc.u-tokyo.ac.jp).

Materials availability

All unique reagents generated in this study are listed in the key resources table and available from the lead contact with a completed Materials Transfer Agreement.

Data and code availability

The results presented in the study are available upon request from the lead contact.

EXPERIMENTAL MODEL AND SUBJECT DETAILS

Cell Culture

HEK293 cells (a human embryonic kidney cell line; ATCC CRL-1573) and HEK293T cells (ATCC CRL-3216) were maintained in Dulbecco's modified Eagle's medium (Sigma-Aldrich) containing fetal calf serum (FCS) and antibiotics. A549 cells (a human lung cell line; ATCC CCL-185) were cultured in Ham's F-12K medium (Thermo Fisher Scientific) with 10% FCS and antibiotics. To generate A549 cells expressing ORF6 upon Dox treatment (Figures 2F and 2G), cells were transduced with a lentiviral vector expressing HA-ORF6 upon Dox stimulation as previously described (Yamada et al., 2018). The pLVX-TetOne-Puro vector expressing GFP (kindly provided by Dr. Nevan J. Krogan) (Gordon et al., 2020) was used as a control. 48 h after lentiviral transduction, the cells were expanded and selected with 1 μg/ml Puromycin (Invivogen, cat# ant-pr-1).

METHOD DETAILS

Viral Genomes and Phylogenetic Analyses

All viral genome sequences used in this study and the respective GenBank or GISAID (https://www.gisaid.org) accession numbers are summarized in Table S1. We aligned the viral genomes and amino acid sequences of *ORF1ab, S, E, M, N* and *ORF6* using the L-INS-i program of MAFFT version 7.453 (Katoh and Standley, 2013). We then constructed phylogenetic trees using the full-length genomes (Figure 1A), *ORF1ab, S, E, M, N* genes (Figure 1B) and *ORF6* gene (Figure 2A). We applied trimAl version 1.4 (Capella-Gutiérrez et al., 2009) with a gappyout option to remove ambiguous alignment regions. For each alignment, we select the best-fit nucleotide and amino acid substitution models using ModelTest-NG version 0.1.5 (Darriba et al., 2020) and selected a General Time Reversible model of nucleotide substitution with invariant sites and gamma distributed rate variation among sites (I+G) for genomes, and LG+I+G for *ORF1ab*, *S*, *E*, and *M* genes, VT+I+G for *N* gene. We then generated a maximum likelihood based phylogenetic tree using RAxML-NG version 1.0.0 (Kozlov et al., 2019) with 1000 bootstrapping tests. We visualized the tree using FigTree software (http://tree.bio.ed.ac.uk/software/figtree).

Plasmid Construction

To construct the expression plasmids for HA-tagged *Sarbecovirus* ORF6 proteins and IAV A/Puerto Rico/8/34 (H1N1 PR8; GenBank accession number EF467817.1) NS1, pCAGGS (Niwa et al., 1991) was used as a backbone. The HA-tagged *Sarbecovirus* ORF6s (the accession numbers and sequences are listed in Table S1) were synthesized by a gene synthesis service (Fasmac). The ORF6 derivatives were generated by PCR using PrimeSTAR GXL DNA polymerase (Takara), the synthesized ORFs as templates, and the primers listed in Table S5. The obtained DNA fragments were inserted into pCAGGS via XhoI-BglII. To construct the Dox-inducible expression plasmids for HA-tagged ORF6, pLVX-TetOne-Puro (Takara, cat# 631849) was used as a backbone. The HA-ORF6 sequences were

generated by PCR using PrimeSTAR GXL DNA polymerase (Takara), the synthesized ORF6s as templates, and the primers listed in Table S5. The obtained DNA fragments were digested with EcoRI and BglII, and were inserted into the EcoRI-BamHI site of pLVX-TetOne-Puro. To construct a Flag-tagged RAE1 expression plasmid, pcDNA3.1 (Thermo Fisher Scientific) was used as a backbone. The Flag-tagged RAE1 sequence was generated by PCR using PrimeSTAR GXL DNA polymerase (Takara), human cDNA, which was synthesized using HEK293-derived mRNA as the template, and the primers listed in Table S5. The obtained DNA fragments were digested with EcoRV and NotI, and inserted into the EcoRV-NotI site of pcDNA3.1. The HA-tagged NUP98 expression plasmid was described in a previous study (Ebina et al., 2004). Nucleotide sequences were determined by a DNA sequencing service (Fasmac), and the sequence data were analyzed by Sequencher version 5.1 software (Gene Codes Corporation).

Transfection, Dox Treatment, IFN treatment and SeV Infection

HEK293 cells were transfected using PEI Max (Polysciences) according to the manufacturer's protocol. For immunofluorescence staining, HEK293T cells were transfected using calcium phosphate as previously described (Langer et al., 2019). For western blotting, cells (in 12 well) were cotransfected with the pCAGGS-based HA-tagged expression plasmids (100, 300 or 500 ng for Figures 2B and S1C; 100 ng for Figures 3B and 3D; 100 or 300 ng for Figure 3G) together with an empty vector (normalized to 1 μg per well). For real-time RT-PCR, cells (in 12 well) were transfected the pCAGGS-based HA-tagged expression plasmids or empty vector (1,000 ng for Figures 2D and 2E). For luciferase reporter assay, cells (in 96 well) were cotransfected with 50 ng of either p125Luc (expressing firefly luciferase driven by human *IFNB1* promoter; kindly provided by Dr. Takashi Fujita) (Fujita et al., 1993) or pISRE-Luc (expressing firefly luciferase driven by human ISRE promoter; kindly provided by Dr. Karl-Klaus Conzelmann) (Brzózka et al., 2006) and the pCAGGS-based HA-tagged expression plasmid (10, 30 or 50 ng for Figures 2C and S1D; 10 ng for Figures 3C, 3E, S2B, and S2C; 10 or 30 ng for Figures 3H and S2D; 30 ng for Figure S1A). The amounts of transfected plasmids were normalized to 100 ng per well. For the compensation assay (Figures 3L and 3M), cells (in 12 well) were cotransfected with the pCAGGS-based SARS-CoV-2 ORF6 expression plasmid (100 ng) and 100, 200 or 400 ng of Flag-tagged RAE1 expression plasmid and 100, 200 or 400 ng of HA-tagged NUP98 expression plasmid (kindly provided by Dr. Yoshio Koyanagi). The amounts of transfected plasmids were normalized to 1,000 ng per well. To induce ORF6-HA expression in A549 cells (described above), they were treated with 1 μg/ml Dox (Takara). At 24 h post transfection or Dox treatment, SeV (strain Cantell, clone cCdi; GenBank accession number AB855654) (Yoshida et al., 2018) was inoculated into the transfected cells at multiplicity of infection (MOI) 10, or IFN-α (100 unit/mL) (PBL Assay Science) or IFN-λ3 (100 ng/ml) (R&D Systems) were treated. In Figure S1A, Ivermectin (Merck) or Selinexor (Selleck Chemicals) (solved with DMSO) was added at 24 h post transfection. For co-IP, HEK293 cells were transfected with pCAGGS-based HA-tagged ORF6 expression plasmids (20 μg, Figure 3I) were transfected into HEK293 cells (in 10-cm dishes) as described above.

Reporter Assay

The luciferase reporter assay was performed 24 h post infection as previously described (Kobayashi et al., 2014; Konno et al., 2018, 2020; Ueda et al., 2017). Briefly, 50 μL cell lysate was applied to a 96-well plate (Nunc), and the firefly luciferase activity was measured using a PicaGene BrillianStar-LT luciferase assay system (Toyo-b-net), and the input for the luciferase assay was normalized by using a CellTiter-Glo 2.0 assay kit (Promega) following the manufacturers' instructions. For this assay, a GloMax Explorer Multimode Microplate Reader 3500 (Promega) was used.

Western Blotting

Transfected cells were lysed with 1x SDS sample buffer (62.5 mM Tris-HCl [pH6.8], 2% SDS, 10% glycerol, 5% 2-mercaptoethanol and 0.0025% bromophenol blue) or RIPA buffer (25 mM HEPES [pH 7.4], 50 mM NaCl, 1 mM $MgCl_2$, 50 μM $ZnCl_2$, 10% glycerol, 1% Triton X-100) containing a protease inhibitor cocktail (Roche). Western blotting was performed as described (Kobayashi et al., 2014; Konno et al., 2018, 2020; Nakano et al., 2017; Yamada et al., 2018) using the antibodies listed in Key resources table.

Co-IP

Co-IP was performed as previously described (Franks et al., 2017; Yoshikawa et al., 2017). Briefly, cells were harvested at 48 h post transfection and lysed with lysis buffer (0.1% Triton X-100, 0.25% sodium deoxycholate, 150 mM NaCl, 1 mM EDTA and 10 mM Tris-HCl [pH 7.5]). The immunoprecipitation was performed using anti-HA magnetic beads (MBL) and western blotting was performed as described above.

Real-time RT-PCR

Real-time RT-PCR was performed as previously described (Konno et al., 2020; Yamada et al., 2018). Briefly, cellular RNA was extracted using QIAamp RNA blood mini kit (QIAGEN) and then treated with RNase-Free DNase Set (QIAGEN). cDNA was synthesized using SuperScript III reverse transcriptase (Thermo Fisher Scientific) and random primer (Thermo Fisher Scientific). Real-time RT-PCR was performed using a Power SYBR Green PCR Master Mix (Thermo Fisher Scientific) and the primers listed in Key resources table. For real-time RT-PCR, a CFX Connect Real-Time PCR Detection System (Bio-Rad) was used.

Immunofluorescence Staining

HEK293T cells were seeded on poly-L-Lysine-coated coverslips in 24-well plates and cotransfected with a SARS-CoV-2 ORF6 expression vector either in combination with RAE1 and NUP98 expression vectors or an empty vector. 16-24 h post transfection, cells were infected with SeV or left untreated. Subsequently, cells were fixed for 20 min at room temperature with 4% paraformaldehyde and permeabilized using PBS containing 0.5% Triton X-100 and 5% FCS for 20 min at room temperature. IRF3 was detected using a unconjugated primary antibody (Cell signaling, dilution 1:200), and fluorophore-conjugated secondary antibody (Thermo Fisher Scientific, dilution 1:1000). Nuclei were visualized by DAPI staining. Cells were mounted in Mowiol mounting medium (Cold Spring Harbor Protocols) and analyzed using confocal microscopy (LSM 710, Zeiss) and the corresponding software (Zeiss Zen Software).

SARS-CoV-2 Sequence Analysis

To survey variants of *ORF6* in pandemic SARS-CoV-2 sequences, we used the viral sequences deposited in GISAID (https://www.gisaid.org) (accessed July 16, 2020). A multiple sequence alignment of SARS-CoV-2 genomes was performed to obtain *ORF6* regions. We first excluded viral genomes that contain undetermined and/or mixed nucleotides in the *ORF6* region. We identified the variants containing shortened coding sequences of *ORF6* as a result of frameshift and/or nonsense mutations. For the sequences, we extracted the information of each GISAID entry, i.e., country, Pangolin lineage, GISAID clade, and sampling date (Table S2). We then clustered the ORF6 mutants when the ORF6 sequences, their Pangolin lineages and GISAID clades were identical. Based on these criteria, 54 clusters were identified (Table S3). To infer the evolutionary dynamics of the ORF6-truncated SARS-CoV-2 mutants, we analyzed 137 SARS-CoV-2 genomes (isolated country, Wales, UK; Pangolin lineage, B.1.5; GISAID clade, G), including 12 ORF6-truncated SARS-CoV-2 mutants in cluster 41 (Table S4). Using these sequences, we generated a multiple sequence alignment using FFT-NS-2 program in MAFFT software version 7.467. We then constructed a maximum likelihood-based phylogenetic tree using RAxML-NG version 1.0.0 with GTR model that was chosen based on AIC values using ModelTest-NG version 0.1.5. We applied a 1,000-time bootstrapping test.

QUANTIFICATION AND STATISTICAL ANALYSIS

Data analyses were performed using Prism 7 (GraphPad Software). The data are presented as averages ± SEM. Statistically significant differences were determined by Student's t test. Statistical details can be found directly in the figures or in the corresponding figure legends.

Cell Reports, Volume *34*

Supplemental information

Sarbecovirus ORF6 proteins hamper induction of interferon signaling

Izumi Kimura, Yoriyuki Konno, Keiya Uriu, Kristina Hopfensperger, Daniel Sauter, So Nakagawa, and Kei Sato

Supplementary Information

Sarbecovirus ORF6 proteins hamper the induction of interferon signaling

Izumi Kimura, Yoriyuki Konno, Keiya Uriu, Kristina Hopfensperger, Daniel Sauter, So Nakagawa, Kei Sato

Supplementary Figures S1-S3
Supplementary Tables S1-S5

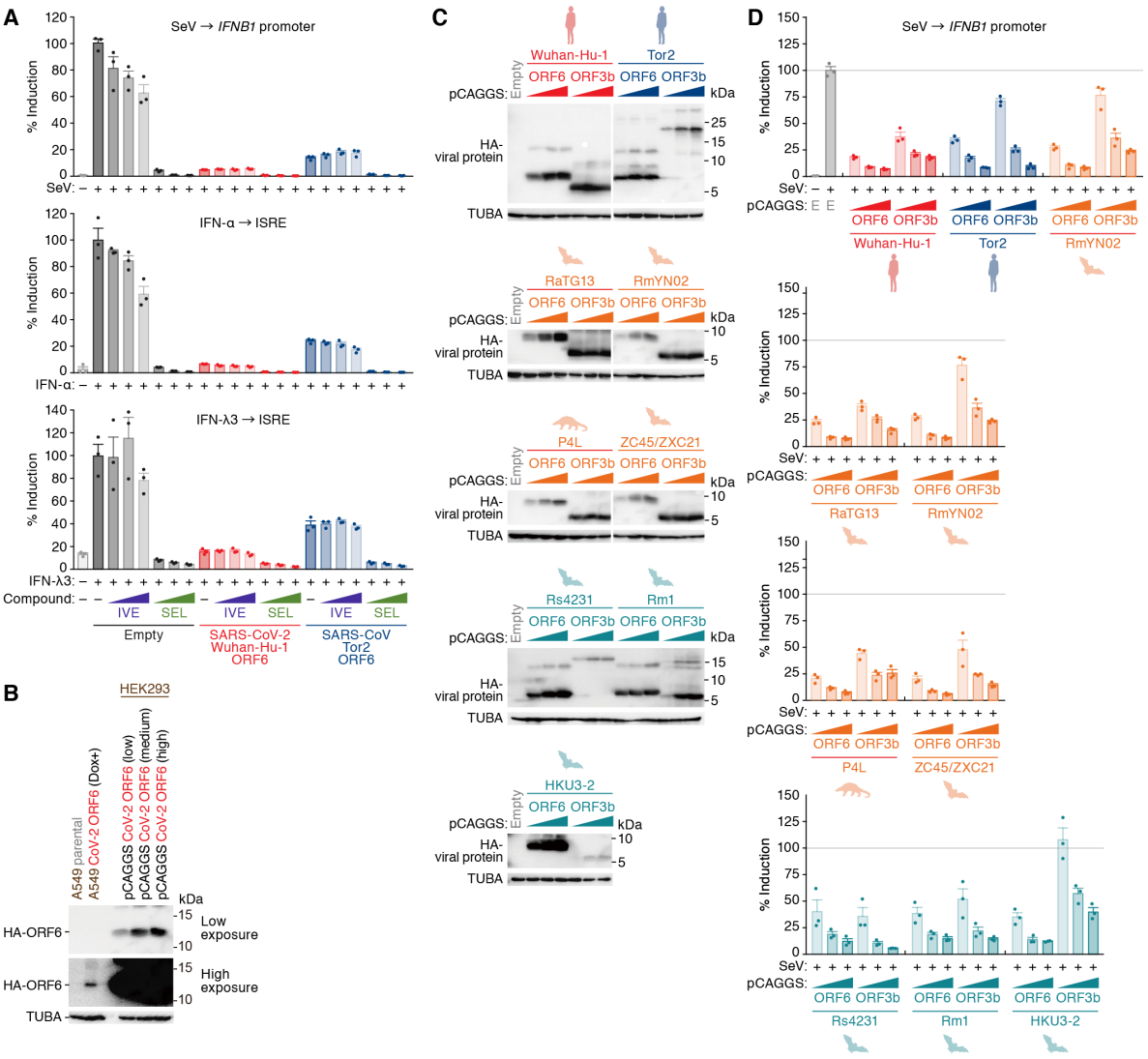

Figure S1. Anti-innate immune signaling activity of *Sarbecovirus* ORF6 (Related to Figure 2).

(**A**) No effects of Ivermectin and Selinexor on the anti-innate immune signaling activity of ORF6. HEK293 cells were cotransfected with plasmids expressing HA-tagged ORF6 proteins of SARS-CoV-2 and SARS-CoV and either p125Luc (top) or pISRE-luc (middle and bottom). 24 h post transfection, cells were infected with SeV (MOI 10) (top), or treated with IFN-α (middle) or IFN-λ3 (bottom) together with three doses of Ivermectin (IVE; 0.2, 1 and 5 μM) or Selinexor (SEL; 0.4, 2 and 10 μM). 24 h post infection or treatment, cells were harvested for luciferase assay.

(**B**) Comparison of ORF6 expression levels in HEK293 cells and A549 cells. To directly compare the expression levels of HA-ORF6 (SARS-CoV-2 strain Wuhan-Hu-1) in HEK293 cells transiently transfected with pCAGGS expression plasmids and those in A549 cells treated with Dox, the cell lysates used in **Figures 2B** and **2F**

were analyzed by Western blotting on the same membrane. To better visualize the bands representing ORF6, blots with lower (top) and higher (bottom) exposures are shown.

(**C** and **D**) Potent anti-IFN activity of *Sarbecovirus* ORF6 and ORF3b. HEK293 cells were cotransfected with three different amounts of plasmids expressing HA-tagged *Sarbecovirus* ORF6 (left) or ORF3b (right) and p125Luc. 24 h post transfection, cells were infected with SeV (MOI 10). 24 h post infection, cells were harvested for Western blotting (**C**) and luciferase assay (**D**).

For Western blotting (**B** and **C**), the input of cell lysate was normalized to TUBA, and one representative result out of three independent experiments is shown. kDa, kilodalton. For the luciferase assay (**A** and **D**), the value was normalized to the unstimulated, empty vector-transfected cells (no SeV infection). E, empty vector.

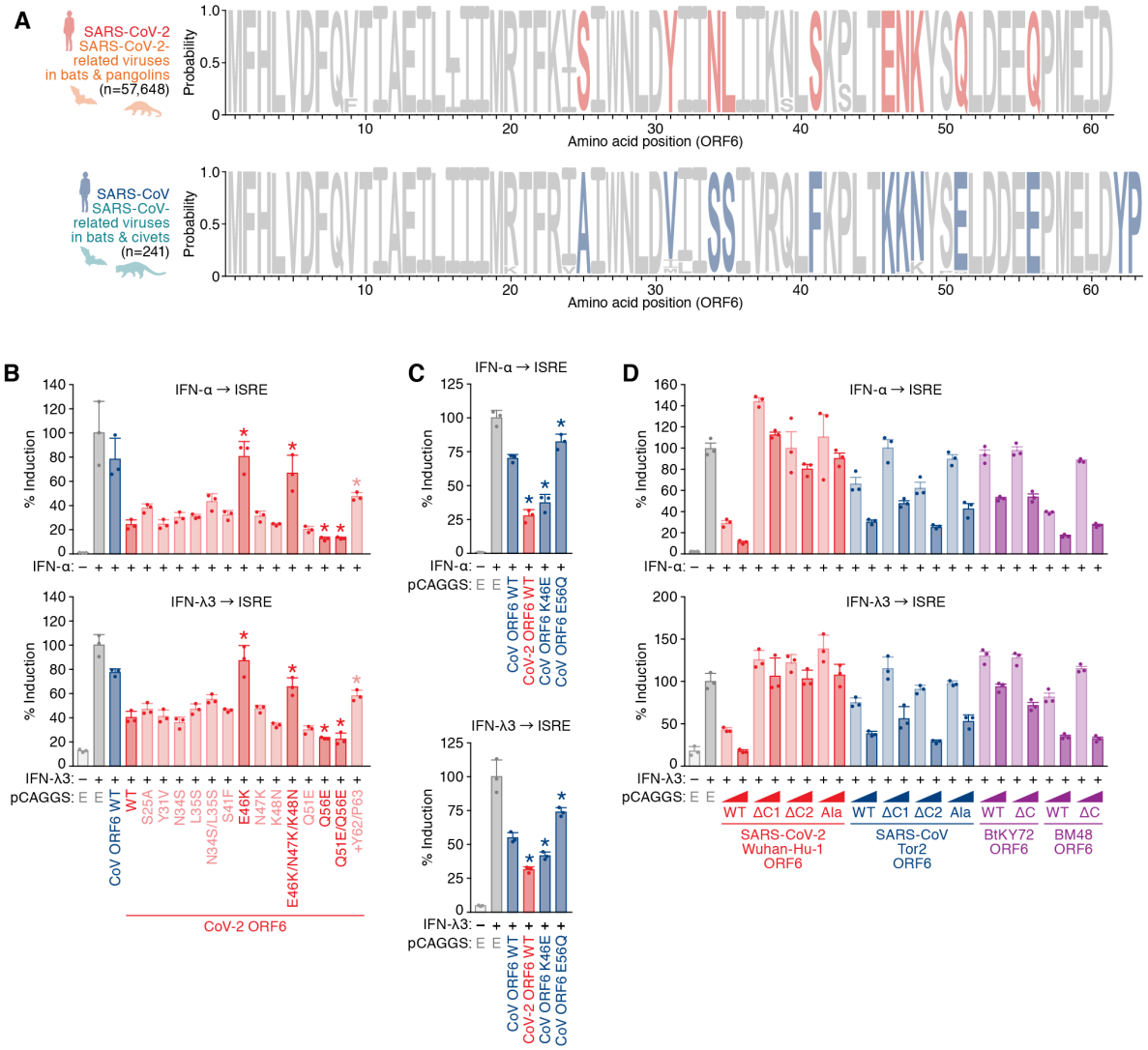

Figure S2. Comparison of the anti-innate immune signaling activities of different *Sarbecovirus* ORF6 proteins (Related to Figure 3).

(**A**) Comparison of ORF6 residues that are different between the SARS-CoV-2 and SARS-CoV lineage. Numbers in parentheses indicate the total number of sequences analyzed. The residues that are different between SARS-CoV-2 (Wuhan-Hu-1) ORF6 and SARS-CoV (Tor2) ORF6 (shown in **Figure 3A**) are shown in color.

(**B** and **C**) Anti-innate immune signaling activity of SARS-CoV-2 ORF6 mutants (**B**) and SARS-CoV ORF6 mutants (**C**). HEK293 cells were cotransfected with plasmids expressing HA-tagged ORF6 variants and pISRE-luc. 24 h post transfection, cells were treated with IFN-α (top) or IFN-λ3 (bottom). 24 h post treatment, cells were harvested for luciferase assay.

(**D**) Anti-innate immune signaling activity of *Sarbecovirus* ORF6 mutants. HEK293 cells were cotransfected with plasmids expressing HA-tagged ORF6 variants and

pISRE-luc. 24 h post transfection, cells were treated with IFN-α (top) or IFN-λ3 (bottom). 24 h post treatment, cells were harvested for luciferase assay.
For the luciferase assay (**B-D**), values were normalized to unstimulated, empty vector-transfected cells (no IFN treatment). In **B**, statistically significant differences ($P < 0.05$) compared to SARS-CoV-2 (Wuhan-Hu-1) ORF6 WT-transfected cells (*) are shown. In **C**, statistically significant differences ($P < 0.05$) compared to SARS-CoV (Tor2) ORF6 WT-transfected cells (*) are shown. E, empty vector.

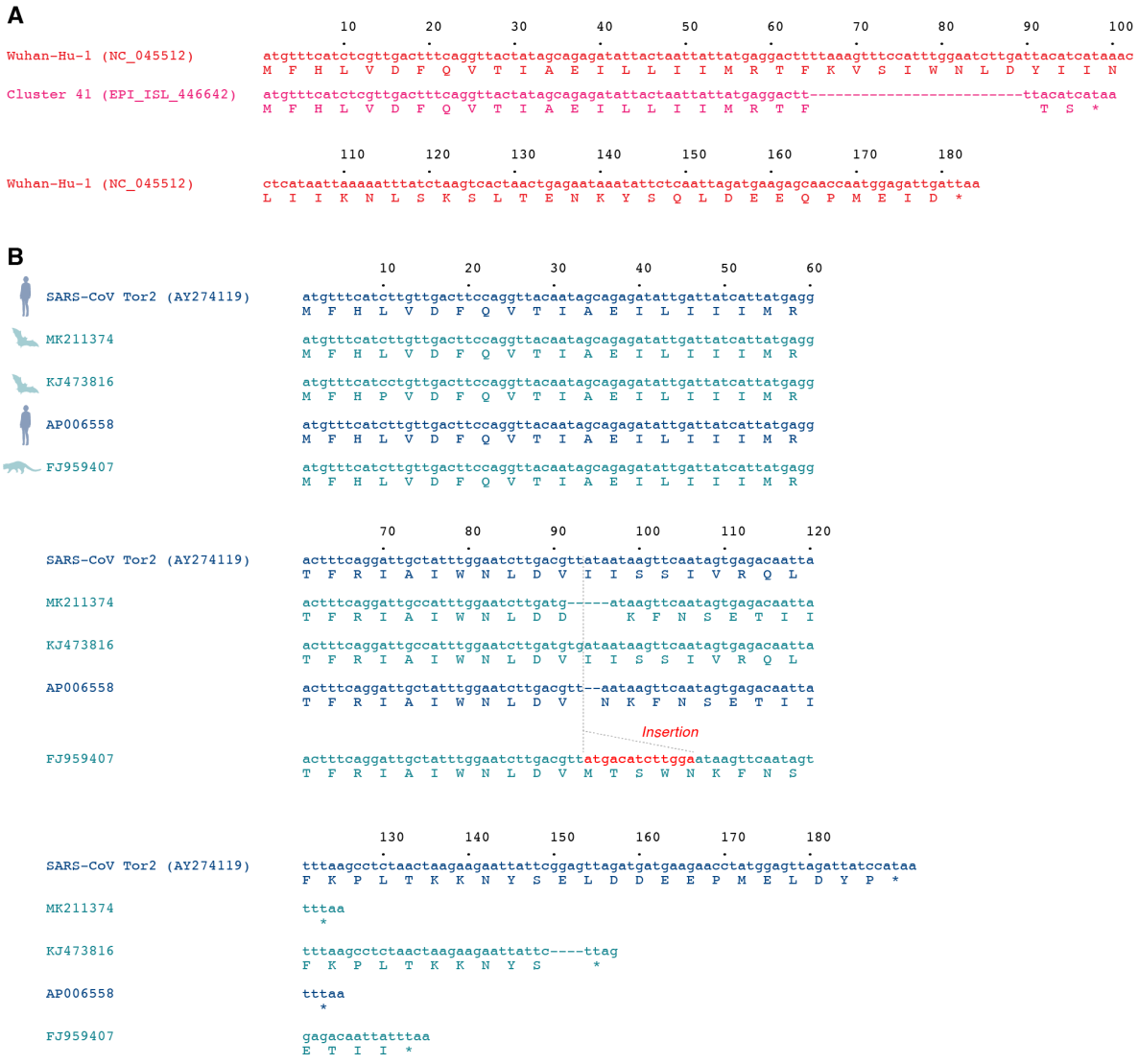

Figure S3. Nucleotide and amino acid sequences of truncated ORF6 (Related to Figure 4)

(**A**) 25-bp deletion of the *ORF6* gene observed in cluster 41. The nucleotide (top) and amino acid sequence (bottom) of SARS-CoV-2 ORF6 (strain Wuhan-Hu-1, GenBank accession number: NC_045512) and that of the truncated ORF6 encoded by the viruses belonging to cluster 41 (**Figure 4B**) are shown. Since all ORF6 sequences of the viruses belonging to cluster 41 are identical, only one representative sequence (GISAID ID: EPI_ISL_446642) is shown.

(**B**) Four frameshift ORF6 mutants the SARS-CoV lineage. The nucleotide (top) and amino acid (bottom) sequence of SARS-CoV ORF6 (strain Tor2, GenBank accession number: AY274119, as the reference) and those of the truncated ORF6 encoded by viruses belonging to the SARS-CoV lineage are shown. For the four

ORF6 frameshift mutants, GenBank accession numbers are indicated. Three of these ORF6 proteins (GenBank accession numbers MK211374, KJ473816 and AP006558) are truncated because of deletions at different regions, while the fourth ORF6 protein (GenBank accession number FJ959407) is truncated due to a frameshift caused by an insertion. MK211374 and KJ473816 are SARS-CoV-related viruses isolated from *Rhinolophus* sp. and *Rhinolophus sinicus*, respectively, while FJ959407 is a SARS-CoV-related virus isolated from a palm civet. AP006558 (strain TWJ) is a human SARS-CoV.